SI Appendix

Trapping the ATP Binding State Leads to a Detailed Understanding of the F_1-ATPase Mechanism

Kwangho Nam,[1,2] Jingzhi Pu,[1,3] and Martin Karplus[1,4]

[1]*Department of Chemistry and Chemical Biology*
Harvard University
12 Oxford Street Cambridge, MA 01238

[2]*Department of Chemistry and Computational Life Science Cluster (CLiC)*
Umeå University
901 87, Umeå, Sweden

[3]*Department of Chemistry and Chemical Biology*
Indiana University-Purdue University Indianapolis (IUPUI)
402 N. Blackford St., LD 326
Indianapolis, IN 46202

and

[4]*Laboratoire de Chimie Biophysique*
Institut de Science et d'Ingénierie Supramoléculaires
Université de Strasbourg
67000 Strasbourg, France

SI1. Structural features of the β_{HC} and β_{HO} conformations.

Based on the B^C angle, each β conformation can be ranked by its "openness" as β_E (48.6°) > β_{HC} (32°) > β_{HO} (23°) > β_{DP} (22°). The B^C helical crossing angle, defined as the angle between the Cα atom positions of helix B (βT163-A176) and helix C (βT190-G204) was determined during the simulation to monitor the opening of the β_{DP} subunit, using the algorithm of Chothia *et al.* (1). Thus, β_{HC} (2) and β_{HO} (3) are placed in-between the "open" β_E conformation and the "closed" β_{DP} conformation. In β_E, additional interactions are formed between β-strand 3 and P-loop and β-strand 7 (βL154/I310, βG156/I310, and βG156/V312; MF_1 numbers are used throughout) upon the disruption of nucleotide binding (4). In β_{DP} and β_{TP}, the closure of the active site is accompanied by the upward domain motions of the C-terminal α-helical domain toward the nucleotide binding domain by approximately 30° from their positions in β_E (5). Not only the difference of the B^C angle, the β_{HC} conformation differs from the reference β_E conformation in the β-sheet twisting angle (52° in β_{HC} and 57° in β_E). This difference appears to be caused by the disruption of the signature H-bond interactions between β-strands 3/7 in β_{HC}.

For β_{HO}, in addition to the slight opening of the binding cleft (B^C angle 23° in β_{HO} versus 21.6° in β_{DP}), the β-sheet is twisted further than that of β_{DP} (β-sheet twisting angle is 37°, compared to 34° in β_{DP}). On the other hand, the helix-6 orientation is similar to that of β_{DP} (H6=48° for β_{HO} and 47° for β_{DP}). This difference suggests that a slight reorientation of the nucleotide binding domain conformation when the partial opening of B^C angle occurs might induce some structural change of neighboring

subunits through the change of the α/β interface interactions but not through the change of the C-terminal domain of β_{DP}, which is consistent with our analysis of cross-correlation maps and structural changes upon ATP hydrolysis in β_{DP} (see the Main Text). We also visually inspected the five known α/β interface conformations, and ranked their the α/β interface openness as $(\alpha/\beta)_{DP} < (\alpha/\beta)_{HO} < (\alpha/\beta)_{TP} < (\alpha/\beta)_{HC} < (\alpha/\beta)_{E}$. This ranking shows that β_{HO} is located between β_{DP} and β_{TP} or β_{HC}. This can be interpreted as that the β_{HO} structure represents a structure along the transition from β_{DP} to β_{HC} or along the transition from β_{TP} and β_{DP}. The former possibility implies the structure is pre-hydrolysis and post-product release conformation, whereas the latter represents the post-ATP binding and pre-hydrolysis conformation. The yeast F_1 crystal structure (3) provides supportive evidence for the first possibility, because the γ-subunit in the β_{HO}-containing yF_1I structure rotates +12° toward the hydrolysis direction compared to the γ-orientation in the reference structure, which has been assigned as the catalytic dwell where hydrolysis takes place in its closed β_{DP} subunit. On the other hand, the latter possibility seems to require a γ-rotation in the opposite direction, i.e., along the synthesis direction, for β_{HO} to be assigned as a pre-hydrolysis intermediate. Our previous analysis is also consistent with the former possibility (6).

SI2. Additional details of the forced rotation simulation

SI2.1. Details of PNM model: In the present work, we have defined two separate plastic networks (6): one for the $\alpha_3\beta3$ crown domain and the other for the γ subunit, respectively, to describe the coupling between the $\alpha_3\beta_3$ and γ networks solely by the all-atom non-

bonded interactions of the CHARMM potential (7). Spring force constants for the crown and γ-stalk networks were set to 500.0 and 2.0 kcal/mol/Å^2, respectively, and the coupling constant for the PNM was set to 1 kcal/mol for both networks. A spherical cutoff of 14 Å was used to define the network connection.

SI2.2. Equilibration details: Starting from a structure that corresponds to the reference Walker structure, the system was first heated from 0 to 300 K in 60 ps, during which each protein backbone atom was harmonically restrained to its crystallographic position. We define the γ rotation angle of the reference Walker structure as 200°, relative to the angle of the ATP binding step at 0° (See Fig. 1B). This makes the 40° rotated ATP waiting state to be at 240°. The system was then subjected to a 300 ps equilibration at 300 K, and the restraints applied to protein backbone atoms were released gradually in the first 40 ps.

SI2.3. Forced rotation simulation: We first determined the (1 ps) update frequency of the force based on the observation that γ rotated at a rate of about 2.5° ps^{-1} in the initial phase of the calculation. The forced rotation simulation was run for 100 ps starting from the β_{DP} conformation. During the simulation, while keeping the external torque, we started inducing the opening of the B^C angle of β_{DP} by the targeted molecular dynamics (TMD) simulation (8), in which the target structure for the β_{DP} opening was generated based on the closed and open structures of β (See Method Section for details of system preparation). The TMD perturbation was applied to the β_{DP} subunit and to the N-terminal β-barrel domain (residues βT9-I84) of β_{DP} and β_E. The inclusion of the N-terminal domains in TMD was necessary to avoid unphysical movement in them. Along with the

β_{DP} opening, the inter-subunit network connections involving β_{DP} (A338-A474) were removed such that the coupling between the β_{DP} subunit and the rest of the crown (mainly through the interface of β_{DP} with the C-terminal domains of α_{DP} and α_{TP}/β_{TP}) is described only by the all-atom CHARMM potential.

In all the forced rotation simulations, we mimicked the His-tag immobilization used in single molecule experiments by harmonically anchoring the center of mass (COM) of the N-terminal β-barrel domains of the three β subunits to the reference structure positions with a force constant of 50 kcal/mol/Å^2. A similar restraint was also added for the COM of the γ-subunit to avoid systematic tilting of the γ-stalk during the forced rotation.

SI2.4. Definition of the γ rotation angle: The γ rotation angles during the simulations were determined as follows. First, a reference vector was computed based on the reference Walker structure (i.e., the hybrid $\alpha_3\beta_3$(1BMF)/γ(1E79) structure), as the projection of the vector connecting Cys78 to the average position between residues 79 ~ 90 of the γ subunit onto the plane defined by residues Ala19 in the three β subunits, which was computed once at the beginning of each simulation and saved. Then, the same definition was used for each simulated structure to compute an instantaneous projection vector. Finally, the γ-orientation angle for each instantaneous structure was computed as the angle formed between the instantaneous vector and the reference vector. The definition used in the present work has been used in the work by Pu and Karplus (6), but using different structure as the reference structure. Similar definition was also used by Koga and Takada (9). Since in the present work we have harmonically restrained the the

$\alpha_3\beta_3$ crown structure, the γ rotation angle determination does not require superposition of the instantaneous structure to the reference structure and thus, mimics closely the single-molecule experiments, such as by Watanabe et al. (10). By contrast, in the work by Cingolani and Duncan (11) and by Okazaki and Takada (12), the γ rotation angles were determined based on superposition of the structure, thus, dependent on how the superposition is carried out.

SI2.5. Alternative protocol for finding the ATP waiting state: To check the results produced from the forced rotation simulation, a protocol was used in the simulation with two modifications. First, the PNM (6) was slightly modified such that the network connections between residues β_{DP}A338-A474, which move significantly as the subunit changes its conformation, and residues from other F_1-crown subunits are removed. Here, we denote the simulation with the alternative protocol as the decoupled network simulation due to the removal of this network connection, whereas the forced rotation simulation described in the Method section is referred to as the coupled network simulation. In the alternative protocol, the coupling in the motion between β_{TP}, β_E and β_{DP} is determined solely by the CHARMM potential. This modification is important, in particular, for understanding the effects of β_{DP} opening on the other parts of the complex. Second, rather than applying a constant torque to induce the γ-rotation, a biasing simulation method (13) was used. In this method, the external torque acts only when γ rotates in the backward (synthesis) direction, and no torque is applied when the rotation is in the forward (hydrolysis) direction.

SI3. Clashes in the forced rotation simulations with a closed β_{DP} conformation.

When an external torque of 5000 pN·nm was applied to the γ-subunit with the β_{DP} subunit remained closed (BˆC = 21.6°), the γ-subunit "stalled" at an angle of about 227° (+27° rotation from the angle at the catalytic dwell). Major clashes between residues γS12-I16 and β_{DP}L384-I388 (located upstream to the β^{394}DELSEED^{400} residues) prevented further rotation (*SI Appendix,* Fig. S1). Another minor clash occurs at the interface between γT20-A27 and α_EA404-A412, a region that contains the loop of the hth motif of α_E , which is also shown in *SI Appendix,* Fig. S1. However, this minor clash disappears when the β_{DP} subunit is open to form the β_E conformation. Thus, it may not contribute significantly on preventing the γ rotation.

SI4. Stabilization of the 240° ATP waiting model structure.

One is a hydrogen bond that replaces the "catch" interactions found in the Walker structure at 200°; i.e., β_ED316, D319 with γR254, Q255 (5). In the ATP waiting state, the hydrogen bonds between β_ED316, D319 and γR254 are disrupted, and the β_ED319/γQ255 hydrogen bond is retained. In addition, a set of new hydrogen bonds are formed between α_ED333, α_ES335 and γR254, which are located near the bifurcating plane of the β_E and β_{DP} subunits, and between β_ED316/γR252, respectively. A close contact between β_{TP}E398 and γR118 is also formed, which contributes in the stabilization of the 240° ATP waiting state (see also *SI Appendix,* Table S1). Since the α_E, β_E, and β_{TP} subunits do not change their conformations significantly, the changes of these hydrogen bonds occur as a consequence of the 40° γ rotation. The simulated ATP waiting state has

a new hydrogen bond between β_{DP}D386, a residue that belongs to the C-terminal hth motif, and γN15; the formation of this hydrogen bond requires a cooperative motion of β_{DP} and γ. During the transition from the closed to the partly open β_{HO}, β_{DP}E395 (part of the conserved β^{394}DELSEED^{400}), which makes a salt-bridge with γR75 in the Walker structure, starts interacting with residue γR133 ionic-track (14); both of these residues are part of the γR133. The corresponding β_{DP}E395:C_β/γR133:C_β distance is shortened from 11.4 Å in the reference structure to 8.5 Å (and the distance of β_{DP}E395:OE2/γR133:NH2 is 2.73 Å) in the simulated 240° state. Since neither pure β_{DP} opening nor pure γ-rotation from the 200° to 240° state is enough to form this salt-bridge, β_{DP}E395/γR133 may play a role in mechanically coupling the two subunits along the rotation to the ATP waiting state.

SI5. Details of explicit water molecular dynamics simulations.

Three catalytic dwell structures and one ATP waiting dwell state structure were prepared based on the procedure described in the Methods section (see the *P_i release simulations* section). The binding pocket of β_{TP} and each α subunit are all occupied by ATP. The β_{DP} and β_E subunits are occupied differently for different systems. The three catalytic dwell states are denoted as the pre-hydrolysis, the post-hydrolysis, and the post-release states, respectively. The two subunits of the pre-hydrolysis state are occupied by ATP and P_i, respectively. In the post-hydrolysis state, the hydrolysis products ADP and P_i occupy the β_{DP} subunit and P_i is still in β_E. Both the post-release state and the ATP waiting state have ADP and P_i in β_{DP} and empty β_E. Each system was then neutralized by adding Na^+ ions (in random positions) and was further solvated with a rhombic

dodecahedron (RHDO) box of 85,041 water molecules, followed by the removal of any water molecules that overlap with the $\alpha_3\beta_3\gamma$ complex and ions, which leaves, for example, 68,273 water molecules and 43 Na^+ ions in the pre-hydrolysis state system.

After 5500 steps of energy minimization to avoid high-energy steric contacts between the protein and water, each system was heated from 8 K to 300 K in 24 ps, followed by 100 ps equilibration at 300 K, during which all protein backbone atoms were harmonically restrained to the corresponding positions of the energy minimized structure. During an additional 100 ps simulation, the harmonic restraints were gradually reduced to zero. The production MD simulations were carried for 20 ns for the ATP waiting dwell state system and 50 ns for the catalytic dwell state systems, respectively. The production MD simulations were carried out using the NAMD program (version 2.8b1) (15). In the simulation, the protein and ions were described by the CHARMM 27 force fields (16) and the CMAP correction for the peptide backbone dihedrals (17), and the water molecules were represented by the TIP3P model (18). The particle mesh Ewald summation (PME) method (19) was used for the evaluation of electrostatics with an approximate grid space of 1.0 Å (150 × 150 × 150 fast Fourier transform grid). The van der Waals interactions were evaluated with a switching function that smoothly transitions the interaction energy to zero between 9 Å and 11 Å. The simulation was carried out with the 2 fs integration time step and SHAKE constraints on bonds involving hydrogen atoms. The temperature of the system was maintained at 300 K using the Langevin thermostat, and the volume of the system was held constant throughout the entire MD simulation.

SI6. Isolated β subunit simulations.

To investigate the mechanism for the partial opening of β_{DP} essential for formation of the ATP waiting state, we have simulated an isolated β subunit with different nucleotide occupancies: MgATP, MgADP+Pi, MgPi, MgADP, and empty. The systems were prepared using the reference β_{DP} subunit structure (PDB ID: 2JDI) (20). Missing residues were added and the ligand coordinates for P_i, ADP, and ATP were modeled into the structure when they were not present in the crystal structure. We assumed that the phosphate groups of ATP and ADP are fully deprotonated in the enzyme and the P_i complexed with ADP is treated as doubly protonated ($H_2PO_4^-$), as used previously (21). Once the initial positions of the ligand atoms and missing residues were modeled, they were minimized with all other atoms of the system held fixed to obtain chemically reasonable starting structures. Each system was then solvated in a periodic boundary water box of $70 \times 70 \times 100$ Å^3, and counter ions (Na^+ and Cl^-) were added to neutralize the system. The potential energy function is the same as the all-atom explicit water $\alpha_3\beta_4\gamma$ simulations, described above, with the PME method for the long range electrostatics. For each system, 12 independent simulations were carried out, each 20 ns in length, starting from different sets of initial velocities. The distribution of B^C angles found in these simulations is shown in *SI Appendix,* Fig. S3A.

The range of values for the isolated subunit are broader than in the crystal structure with the peak in each case at a smaller value than that observed in crystal structure (e.g. the empty subunit has its maximum at around 30°, while the β_E values is 46°). Of most interest is the result that MgADP+Pi and MgPi are significantly more open

than MgATP, suggesting these two occupancies are possible triggers for opening β_{DP} toward β_{HC} or β_{HO}.

Potentials of mean force (PMFs) with the B^C angle and the β-sheet twisting angle as progress variables were obtained by umbrella sampling simulations (22). The B^C angle changes from 16° to 50° and the β-sheet twisting angle (23) varies from 34° in β_{TP} to 57° in β_E, respectively. The β-sheet twisting angle was introduced to describe the hydrogen bond disruptions between the β-strands 3 and 7 upon product release (4). The initial configurations and velocities for each umbrella sampling window were selected along ~400 ps TMD trajectories (RMSD step 0.00002 Å/timestep) that drive the conformational change from β_{DP} to β_E. For each umbrella sampling window, 1 ns MD simulations were carried out with a force constant in the range of 100 to 300 kcal/mol/rad^2. The final PMFs were computed using the Weighted Histogram Analysis Method (24). The results are presented in *SI Appendix*, Fig. S3B.

With MgATP bound (*SI Appendix*, Fig. S3B(a)), a closed conformation (B^C=25°, β-sheet=38°), is found as a single free energy minimum (~4 kcal/mol more stable than the open β_E conformation). With the hydrolysis product MgADP+P_i bound (*SI Appendix*, Fig. S3B(b)), the free energy well is broadened relative to the MgATP occupied subunit, with slightly more population at B^C=30° and β-sheet=38°. Release of P_i with MgADP in the site (*SI Appendix*, Fig. S3B(c)), results in a further broadened free energy minimum at B^C=32°, in a qualitative agreement with the partly open β_{HO} conformation found at the ATP waiting model structure (marked as "o" on *SI Appendix*, Fig. S3B(a)). If MgADP is released before the release of P_i (*SI Appendix*, Fig. S3B(d)), the stable conformations are also shifted toward the open ones (B^C=30°~33°). The second

minimum adopts a β-sheet twisting angle of 50°, in agreement with the β_{HC} conformation (marked as "*" on *SI Appendix,* Fig. S3B(a)). With both ligands released (*SI Appendix,* Fig. S3B(e)), the open conformation (B^C= 40° to 45°, β-sheet=50° to 55°) is ~7 kcal/mol more stable than that of the closed conformation and the subunit becomes most flexible. In addition, a second free energy minimum is found between the partly open β_{DP} conformation and the fully open β_E conformation, suggesting that there is a free energy minimum near the β_{HO} conformation. Very recently, similar results were reported by Czub and Grubmüller (25); they have carried out free energy simulations with an isolated β subunit without bound ligand and found that the half-closed conformation is thermodynamically favored.

The PMF results were used to estimate the change of the relative free energy between the open and closed form of an isolated β-subunit upon ATP binding, which is 11 kcal/mol (compare *SI Appendix*, Figs. S3B(a) and (e)). This value is in good agreement with the value (9.6 kcal/mol) estimated from experimentally measured binding affinities, and provide a good support of our PMF results. In the estimation of the free energy change, we used the experimental binding affinities for MgATP, and assumed that the relative free energy between the β_{DP} and β_{TP} conformations is zero. This is a reasonable approximation, because the closed β_{DP} and β_{TP} conformations are similar to each other and the free energy difference between β_{DP} and β_{TP}, with MgATP bound, is expected to be small. The dissociation constants (K_d) of MgATP from the "tight" (β_{TP}) and "open" (β_E) sites have been measured as 0.2 nM (26) and >10mM (27), and they correspond to -12.4 and -2.8 kcal/mol in free energy, respectively. The difference gives +9.6 kcal/mol as the free energy change.

SI7. Further details of P_i release simulation.

In each MCES simulation, all atoms from the α and β subunits that are not directly involved in P_i release were held fixed to their corresponding starting position: for example, for the release from β_{DP}, the α_{TP}, α_E, $\beta_{TP,}$ and β_E subunits were held fixed, and for the release from β_E site, α_{TP}, α_{DP}, $\beta_{TP,}$ and β_{DP} were held fixed, respectively. In addition, all non-hydrogen atoms of residues γA41-K218 were harmonically restrained to their starting positions. For each P_i temperature, the average release probability was evaluated from 40 independent simulations, which is equivalent to a total of 1200 independent P_i release simulations. A high temperature was applied to P_i to facilitate the escape of it from the binding pocket.

SI8. P_i release pathways.

The P_i release trajectories from β_E (200°) and β_{HO}-like (240°) obtained from the MCES simulations show three different pathways for P_i release (see *SI Appendix*, Fig. S4A and B), although only the front door pathway is significant. In the first path (backdoor I; red), P_i is released through a space between the upper tip of the γ stalk and the $\alpha_3\beta_3$ crown; in the second path (backdoor 2; green), P_i diffuses through a space between the C-terminal domain of the β_E subunit and the lower part of the γ stalk; in the third pathway (front door) P_i exits through an opening present in the β_E structure. In *SI Appendix*, Fig. S4C, we present the probabilities through the dominant pathway for each case along with the total release probabilities. Since backdoor I is rarely used, backdoor II is the only accessible pathway for P_i release when ADP is present and blocks the front

door, as in β_{HO}-like and β_{DP} at 200°. However, the release probability through the backdoor II is very small when ADP is absent so that it is unlikely to contribute significantly to the normal cycle.

SI9. P_i binding modes and conformational change.

It has been proposed that β_E undergoes a structural rearrangement to produce the power stroke for γ rotation (10, 28). To obtain hints concerning the conformational change, various β_E crystal structures with and without P_i in the binding pocket were compared (*SI Appendix,* Fig. S10). The comparison reveals no difference in the structure between the β_E structures with or without P_i, except a relatively small displacement of the P-loop for the structure of P_i (*SI Appendix,* Fig. S10B). In addition, we found two binding modes of P_i in β_E: one binds in the P-loop and the other binds further inside and interacts with β_EN257 and β_ER189. This finding is similar to the results of structural comparisons by Okazaki and Takada (12). The two sites have some similarity to the binding sites of ADP and P_i in β_{DP}, respectively. The β–phosphate of ADP binds in the P-loop, and P_i (or its analog) binds inside (but not as deep as the P_i in the second site of β_E) and interacts with βN257 and βR189, respectively (*SI Appendix,* Fig. S12). In β_{TP}, although the β–phosphate of ATP binds in the P-loop, the terminal phosphate binds between the P-loop and the P_i site in β_{DP} and interacts only with βR189 (*SI Appendix,* Fig. S12B). The differences of the binding modes between P_i, ADP, and ATP suggest that the P-loop is the preferred binding site for P_i. The comparison also suggests that the P_i cleaved from ATP translocates to the second binding site, which could contribute to the conformational change in β_{DP} during the γ rotation.

SI10. Test of the ATP waiting state model by S-S cross-linking data and FRET measurements.

Support for the conformation of the ATP-waiting state proposed here is provided by existing cross-linking data. Sielaff *et al*. (29) demonstrated that for EcF_1-ATPase residues αE284C/γQ274C (MF_1:αE292C/γK260C) can be cross-linked and fix the γ-subunit at 0° from the MgADP inhibited dwell, which was assigned to the reference structure. In the simulated 240° structure, the C_β-C_β distance between γK260 and α_{TP}E292 is significantly shorter (8.0 Å), compared with that in the reference structure (9.5 Å). Interestingly, the distance between γK260 and α_{DP}E292 is slightly shorter (9.3 Å) than that of α_{TP}E292 in the reference structure; the corresponding C_β-C_β distances averaged over seven crystal structures 1BMF, 1E79, 1H8E, 1W0J, 2JDI, 2CK3, and 1E1R) are 10.1±0.1 Å and 8.9±0.2 Å, for α_{TP}E292/γK260 and α_{DP}E292/γK260, respectively.

Okuno *et al*. (30) reported that the disulfide bond introduced in TF_1:$\alpha_3\beta_2\beta$(E190D/E391C)/γ(R84C) (in MF_1, $\alpha_3\beta_2\beta$(E188D/E395C)/γ(R75C)) can lock the enzyme at the catalytic dwell, in which the slow β mutant β(E188D) was assigned to adopt a closed β_{DP} conformation. This is consistent with various MF_1 crystal structures. The average crystallographic C_γ-C_γ distance of β_{DP}E395/γR75 is 5.9±0.2 Å, see Table 1 of Okuno et al. (30), and the averaged crystallographic C_β-C_β distance is 8.3±0.2 Å, respectively. In the yeast MF_1 crystal structure (yF_1I, PDB:2HLD) that contains a β_{HO} conformation (3), the C_γ-C_γ distance of yF_1: β_{HO}E395/γK81 is 8.3 Å (the C_β-C_β distance is 8.9 Å), much longer than that observed in MF_1 structures but shorter than the distance in the simulated 240° structure (the C_γ-C_γ distance of β_{DP}E395/γR75 is 11.1 Å and the C_β-

C_β distance is 12.8 Å). These results suggest that the β_{HO} conformation of yF_1I structure is in-between the catalytic dwell and the ATP-waiting states.

Early FRET measurement of Yasuda *et al*. (31) concluded that in the ATP-waiting state the TF_1:βS205C/γS107C (MF_1:βS203/γA99) distances are equal to 57±10, 79±10, and 79±10 Å, respectively for three β/γ combinations. In the simulated 240° structure, the C_α-C_α distances of β_{TP}S203, β_{DP}S203, and β_ES203, from γA99 are 61, 89, and 93 Å, respectively. These distances are in good agreement with the short/long/long combination pattern observed in the FRET experiment (31), given that the FRET measurements are only qualitative because of the use of large reporter groups (29).

SI11. Possible Additional S-S crosslinks to trap the ATP waiting state.

To identify additional cross-linking sites involving the γ-subunit and the surrounding crown subunits, we introduced a criterion that combines the ratio of the ensemble averaged C_β-C_β distance from MD simulations at the 240° state ($\langle r_1 \rangle$) vs. that at the reference structure (r_2) and the C_β-C_β distance itself. We note that our distance criterion is slightly longer than the C_β-C_β distance criterion normally used for the S-S pair design ($\leq$ 4.6 Å) (32). Since protein local structure often changes, such as by side chain rotation, to accommodate the mutated residue, we allowed the longer distance criterion to expand the search space for the potential cross-linking sites. The candidate S-S pairs were then ranked by a scoring function in which the two parameters are equally weighted; top scorers are listed below in *SI Appendix*, Table S1, in which recommended cross-linking sites are high-lighted in bold. Given that the proposed β_{DP} partly opening is coupled with the 40° rotation, the β_{DP}/γ S-S locks (the ones that are absent in the

reference 200° state) are particularly important. A suggested example involves the contact between β_{DP}D386 and γI19; the C_β-C_β distance changes from 11.5 Å in the reference structure to 7.0 Å in the 240° state. Another possibility arises from the fact that the γ rotation makes the contacts between β_{DP}276-280 and γ258-262 closer. As a result, the C_β-C_β distance between β_{DP}V279 and γI258 is shortened from 12.1 Å in the reference structure to 7.4 Å in the 240° state.

Use of a β_{DP} residue to form a S-S bond to the γ subunit is of particular interest because introduction of double mutations of the β_{DP} subunit makes it possible to identify the 240° state by a single-molecule rotation assay (30). A hybrid enzyme with the E190D mutation and the cysteine mutation in the same β_{DP} subunit could be used, together with two wild type β subunits. The consequent β_2(WT)β(E190D,V279C) species can be identified by picking the chimera enzyme with the prolonged catalytic dwell. Then the proposed S-S lock can be introduced by oxidation. (It will be between β_{DP}(V279C) and γ, since βE190D adopts a β_{DP}-like conformation at the prolonged catalytic dwell.) The proposed S-S lock is expected to halt the enzyme at 240° (i.e., in the ATP waiting state) as compared to the prolonged catalytic dwell γ-orientation.

Other S-S pairs that do not directly involve the proposed partly open β_{HO} conformation can be made as well to attempt to trap the ATP-waiting state; these sites include β_{TP}D394/γG76, β_{TP}E398/γS114, β_ED316/γR252, α_{DP}D333/γK4, α_{TP}R286/γA270, and α_ES408/γA29 (*SI Appendix*, Table S1). These sites are selected based on the fact that during the 40° rotation, the major change occurs in the γ orientation, while the $\alpha_3\beta_3$ exhibits only minor structural changes. In addition, since the introduced mutation will likely be included in all three β (or three α) subunits in the cross-linking experiments, it is

important to avoid forming a cross-link between unwanted subunits. Therefore, we have identified the listed sites to ensure that only the indicated pairs of subunits can be cross-linked at a given state, while the other two subunits cannot be cross-linked with the γ subunit (i.e., mainly due to the long distances between the corresponding residues in β (or α) and the residue in γ). We present two examples of the proposed disulfide cross-linking sites in *SI Appendix*, Fig. S13. In the figure, the pairs of residues (i.e., β_{TP}D394/γG76 and β_{TP}E398/γS114) are compared between the reference catalytic dwell structure at 200º and the modeled 240º ATP waiting state structure. Since the γ-protrusion region has to pass through the C-terminal domain of β_{TP} during the 120º γ rotation (from 200º to 240º, and to 320º), the proposed cross-linking sites are well positioned for trapping the ATP waiting state experimentally and crystallizing the ATP waiting state. In particular, as shown in *SI Appendix*, Fig. S13, the protruded part of the γ subunit have direct contacts with the C-terminal domain of β_{TP} subunit at 240º model structure.

References

1. Chothia C, Levitt M, Richardson D (1981) Helix to helix packing in proteins. *J Mol Biol* 145:215-250.

2. Menz RI, Walker JE, Leslie AGW (2001) Structure of bovine mitochondrial F_1-ATPase with nucleotide bound to all three catalytic sites: Implications for the mechanism of rotary catalysis. *Cell* 106:331-341.

3. Kabaleeswaran V, Puri N, Walker JE, Leslie AGW, Mueller DM (2006) Novel features of the rotary catalytic mechanism revealed in the structure of yeast F_1 ATPase. *EMBO J* 25:5433-5442.

4. Yagi H, Kajiwara N, Iwabuchi T, Izumi K, Yoshida M, Akutsu H (2009) Stepwise propagation of the ATP-induced conformational change of the F_1-ATPase β subunit revealed by NMR. *J Biol Chem* 284:2374-2382.

5. Abrahams JP, Leslie AGW, Lutter R, Walker JE (1994) Structure at 2.8 Å resolution of F_1-ATPase from bovine heart mitochondria. *Nature* 370:621-628.

6. Pu J. Karplus K (2008) How subunit coupling produces the γ-subunit rotary motion in F_1-ATPase. *Proc Natl Acad Sci USA* 105:1192-1197.

7. Brooks BR, Bruccoleri RE, Olafson BD, States DJ, Swaminathan S, Karplus M (1983) CHARMM: A program for macromolecular energy, minimization, and dynamics calculations. *J Comput Chem* 4:187-217.

8. Schlitter J, Engels M, Krüger P, Jacoby E, Wollmer A (1993) Targeted molecular dynamics simulation of conformational change-Application to the T ↔ R transition in insulin. *Mol Simul* 10:291-308.

9. Koga N, Takada, S. (2006) Folding-based Molecular Simulations Reveal Mechanisms of the Rotary Motor F_1-ATPase. *Proc Natl Acad Sci USA* 103:5367-5372.

10. Watanabe R, Iino R, Noji H. (2010) Phosphate release in F_1-ATPase catalytic cycle follows ADP release. *Nat Chem Biol* 6:814-820.

11. Cingolani, G, Duncan, TM (2011) Structure of the ATP Synthase Catalytic Complex (F_1) from *Escherichia coli* in an Autoinhibited Conformation. *Nat Struct Mol Biol* 18:701-707.

12. Okazaki K, Takada S (2011) Structural comparison of F_1-ATPase: Interplay among enzyme structures, catalysis, and rotations. *Structure* 19:588-598.

13. Paci E, Karplus M (1999) Forced unfolding of fibronectin type 3 modules: an analysis by biased molecular dynamics simulations. *J Mol Biol* 288:441-459.

14. Ma J, Flynn TC, Cui Q, Leslie AGW, Walker JE, Karplus M (2002) A dynamic analysis of the rotation mechanism for conformational change in F_1-ATPase. *Structure* 10:921-931.

15. Kalé L, Skeel R, Bhandarkar M, Brunner R, Gursoy A, Krawetz N, Phillips J, Shinozaki A, Varadarajan A, Schulten K (1999) NAMD2: Greater scalability for parallel molecular dynamics. *J Comput Phys* 151:283-312.

16. MacKerell AD, Jr, Bashford D, Bellott M, Dunbrack RL, Jr, Evanseck JD, Field MJ, Fischer S, Gao J, Guo H, Ha S, Joseph-McCarthy D, Kuchnir L, Kuczera K, Lau FTK, Mattos C, Michnick S, Ngo T, Nguyen DT, Prodhom B, Reiher WE, III, Roux B, Schlenkrich M, Smith JC, Stote R, Straub J, Watanabe M, Wiórkiewicz-Kuczera J, Yin D, Karplus M (1998) All-atom empirical potential for molecular modeling and dynamics studies of proteins. *J Phys Chem B* 102:3586-3616.

17. MacKerell AD, Jr, Feig M, and, Brooks CL, III (2004) Improved treatment of the protein backbone in empirical force fields. *J Am Chem Soc* 126:698-699.

18. Jorgensen WL, Chandrasekhar J, Madura JD, Impey RW, Klein ML (1983) Comparison of simple potential functions for simulating liquid water. *J Chem Phys* 79:926-935.

19. Darden T, York D, Pedersen L (1993) Particle mesh Ewald: An N·log(N) method for Ewald sums in large systems. *J Chem Phys* 98:10089-10092.

20. Bowler MW, Montgomery MG, Leslie AGW, Walker JE (2007) Ground state structure of F_1-ATPase from bovine heart mitochondria at 1.9 Å resolution. *J Biol Chem* 282:14238-14242.

21. Yang W, Gao YQ, Cui Q, Ma J, Karplus M (2003) The missing link between thermodynamics and structure in F_1-ATPase. *Proc Natl Acad Sci USA* 100:874-879.

22. Torrie GM, Valleau JP (1977) Nonphysical sampling distributions in Monte Carlo free-energy estimation: Umbrella sampling. *J Comput Phys* 23:187-199.

23. Sun S, Chandler D, Dinner AR, Oster G (2003) Elastic energy storage in β-sheets with application to F_1-ATPase. *Eur Biophys J* 32:676-683.

24. Kumar S, Rosenberg JM, Bouzida D, Swendsen RH, Kollman PA (1992) The weighted histogram analysis method for free-energy calculations on biomolecules. I. The method. *J Comput Chem* 13:1011-1021.

25. Czub J, Grubmüller H (2014) Rotation triggers nucleotide-independent conformational transition of the empty β subunit of F_1-ATPase. *J Am Chem Soc* 136:6960-6968.

26. Gao YQ, Yang W, Marcus RA, Karplus M (2003) A model for the cooperative free energy transduction and kinetics of ATP hydrolysis by F_1-ATPase. *Proc Natl Acad Sci USA* 100:11339.

27. Senior AE, Nadanaciva S, Weber J (2002) The molecular mechanism of ATP synthesis by F_1F_0-ATP synthase. *Biochim Biophys Acta* 1553:188-211.

28. Masaike T, Koyama-Horibe F, Oiwa K, Yoshida M, Nishizaka T (2008) Cooperative three-step motions in catalytic subunits of F_1-ATPase correlate with 80° and 40° substep rotations. *Nat Struct Mol Biol* 15:1326-1333.

29. Sielaff H, Rennekamp H, Engelbrecht S, Junge W (2008) Functional halt positions of rotary F_OF_1-ATPase correlated with crystal structures. *Biophys J* 95:4979-4987.

30. Okuno D, Fujisawa R, Iino R, Hirono-Hara Y, Imamura H, Noji H (2008) Correlation between the conformational states of F_1-ATPase as determined from its

crystal structure and single-molecule rotation. *Proc Natl Acad Sci USA* 105: 20722-20727.

31. Yasuda R, Masaike T, Adachi K, Noji H, Itoh H, Kinosita K, Jr (2003) The ATP-waiting conformation of rotating F_1-ATPase revealed by single-pair fluorescence resonance energy transfer. *Proc Natl Acad Sci USA* 100:9314-9318.

32. Hazes B, Dijkstra BW (1988) Model building of disulfide bonds in proteins with known three-dimensional structure. *Protein Eng* 2:119-125.

33. Rees DM, Montgomery MG, Leslie AGW, Walker JE (2012) Structural evidence of a new catalytic intermediate in the pathway of ATP hydrolysis by F_1–ATPase from bovine heart mitochondria. *Proc Natl Acad Sci USA* 109:11139-11143.

34. Braig K, Menz RI, Montgomery MG, Leslie AGW, Walker JE (2000) Structure of bovine mitochondrial F_1-ATPase inhibited by Mg^{2+}ADP and aluminium fluoride. *Structure* 8:567-573.

35. Gibbons C, Montgomery MG, Leslie AGW, Walker JE (2000) The structure of the central stalk in bovine F_1-ATPase at 2.4 Å resolution. *Nat Struct Biol* 7:1055-1061.

TABLE S1. β(or α)/γ residue C_β-C_β distances[a] at the 240° ATP waiting state and the 200° reference structures, in which recommended cross-linking sites are highlighted with bold.

α/β-residue	γ-residue	240° (ATP-waiting, $<r_1>$[b])	Reference (1BMF+1E79, r_2)	$<r_2>$[c]	Ratio ($<r_1>/r_2$)	Score[d]
β_{DP}	**γ**					
D386	**I19**	7.04±0.27	11.54	11.59±0.36	0.61	100.0
V279	**I258**	7.44±0.28	12.12	12.46±0.19	0.61	97.0
A278	I258	7.29±0.35	10.09	10.69±0.28	0.72	90.5
I387	S22	8.49±0.23	12.40	12.64±0.57	0.69	86.0
G280	E261	7.30±0.20	8.83	9.00±0.24	0.83	85.1
β_{TP}	**γ**					
E398	**S114**	4.96±0.33	13.31	12.99±0.38	0.37	98.8
I275	G268	4.85±0.18	6.68	8.03±0.07	0.73	75.7
S397	S114	6.56±0.34	12.48	11.50±1.20	0.53	72.4
D394	**G76**	5.69±0.21	9.01	10.21±0.27	0.63	72.1
E398	R118[e]	7.14±0.22	12.72	13.53[f]	0.61	67.2
β_{E}	**γ**					
D316	**R252**	5.72±0.23	8.88	9.45±0.12	0.64	95.1
D316	L248	5.89±0.27	8.70	9.48±0.26	0.68	91.5
D315	L248	6.98±0.31	10.60	12.15±0.32	0.66	85.1
E395	S167	8.82±0.67	15.07	19.07±2.86	0.59	82.0
P276	I263	6.75±0.25	9.09	8.64±0.23	0.74	81.5
L391	V168	8.04±0.58	12.34	14.69±2.82	0.65	80.1
α_{DP}	**γ**					
D333[g]	**K4**	5.28±0.18	12.13	12.87±1.35	0.44	100.0
A336	K4	7.62±0.23	13.84	14.04±1.11	0.55	89.6
D331	K4	8.20±0.29	14.74	15.76±1.27	0.56	89.1
D331	D5	6.72±0.21	11.82	12.39±1.16	0.57	88.3
E292	E261	7.42±0.21	9.74	10.54±0.18	0.76	78.6

α_{TP}	γ					
R286	**A270**	6.01±0.22	7.24	7.24±0.22	0.83	86.8
P289	S267	6.54±0.20	8.38	8.88±0.20	0.78	85.1
A293	K260	7.82±0.27	9.36	9.71±0.11	0.84	75.0
E292[h]	K260[h]	7.97±0.24	9.45	10.09±0.12	0.84	74.0
α_{E}	γ					
F406	M25	5.58±0.30	12.27	12.27±0.59	0.45	94.0
G407	M25	5.46±0.42	10.91	10.84±0.82	0.50	90.3
S408	**A29**	4.91±0.58	12.17	12.55±0.79	0.58	89.0
F403	M25	5.54±0.31	9.67	10.42±1.34	0.57	84.0
F406	V26	5.59±0.27	9.61	9.67±0.62	0.58	83.1

[a]In Å; Cα atom coordinate is used for Gly.
[b]Averaged values based on 400 ps MD simulations ± standard deviations.
[c]Averaged values (when coordinates are available) based on seven crystal structures, i.e., 1BMF (1), 1E79 (2), 1H8E (3), 1W0J (4), 2JDI (5), 2CK3 (6), and 1E1R (7); ± standard deviations.
[d]Scores are calculated by $[\langle r_1 \rangle_{min}/r_1 + (\langle r_1 \rangle/r_2)_{min}/(\langle r_1 \rangle/r_2)] / 2 \times 100$, where $\langle r_1 \rangle_{min}$ and $(\langle r_1 \rangle/r_2)_{min}$ represent the minimal values of $\langle r_1 \rangle$ and $\langle r_1 \rangle/r_2$ among the listed S-S pairs for each α/γ or β/γ group.
[e]Residues that belong to the "ionic track" (8).
[f]Only available in the 1E79 crystal structure.
[g]αD333 was also mutated in one of Sielaff et al.'s S-S pairs, i.e., EcF_1:αD336C/γK266C (or MF_1:αD333C/γR252C); the disulfide bond locks the γ-subunit at 305° (or 185°) (9).
[h]Sielaff et al.'s S-S pair, i.e., EcF_1:α284C/γQ274C (or MF_1:αE292C/γK260C), that blocks the rotation at 240°.

References

1. Abrahams JP, Leslie AGW, Lutter R, Walker JE (1994) Structure at 2.8 Å resolution of F_1-ATPase from bovine heart mitochondria. *Nature* 370:621-628.

2. Gibbons C, Montgomery MG, Leslie AGW, Walker JE (2000) The structure of the central stalk in bovine F_1-ATPase at 2.4 Å resolution. *Nat Struct Biol* 7:1055-1061.

3. Menz RI, Walker JE, Leslie AGW (2001) Structure of bovine mitochondrial F_1-ATPase with nucleotide bound to all three catalytic sites: Implications for the mechanism of rotary catalysis. *Cell* 106:331-341.

4. Kagawa R, Montgomery MG, Braig K, Leslie AGW, Walker JE (2004) The structure of bovine F_1-ATPase inhibited and beryllium fluoride. *EMBO J* 23:2734-2744.

5. Bowler MW, Montgomery MG, Leslie AGW, Walker JE (2007) Ground state structure of F_1-ATPase from bovine heart mitochondria at 1.9 Å resolution. *J Biol Chem* 282:14238-14242.

6. Bowler MW, Montgomery MG, Leslie AGW, Walker JE (2006) How azide inhibits ATP hydrolysis by the F-ATPases. *Proc Natl Acad Sci USA* 103:8646-8649.

7. Braig K, Menz RI, Montgomery MG, Leslie AGW, Walker JE (2000) Structure of bovine mitochondrial F_1-ATPase inhibited by Mg^{2+}ADP and aluminium fluoride. *Structure* 8:567-573.

8. Ma J, Flynn TC, Cui Q, Leslie AGW, Walker JE, Karplus M (2002) A dynamic analysis of the rotation mechanism for conformational change in F_1-ATPase. *Structure* 10:921-931.

9. Sielaff H, Rennekamp H, Engelbrecht S, Junge W (2008) Functional halt positions of rotary F_OF_1-ATPase correlated with crystal structures. *Biophys J* 95:4979-4987.

Supplemental Figure Captions

Figure S1. Clashes developed during the pulling simulations with the reference Walker crown conformation. The γ-stalk (purple) rotation is stalled at 220° even in the presence of a large torque. There is a major clash at the interface of β_{DP} (L384-I388/γS12-I16) and a minor clash at α_E (A404-A412/γT20-A27). The major clash is removed when the β_{DP} subunit opens further so that forced rotation can resume. Color scheme: β_{DP}, α_E, and γ are in orange, blue, and purple, respectively.

Figure S2. Structural analyses of all-atom explicit water MD simulations. (A) The structure of the model ATP waiting state obtained from all-atom explicit water molecular dynamics (MD) simulations is overlaid on the catalytic dwell state structure (gray color). For clarity, only β_E (yellow), β_{DP} (orange), and γ (purple) subunits are shown. The B and C helices are shown in blue. The structure shows the rotation of the γ subunit, the partial opening of the C-terminal domain of β_{DP}, and the slight closure of the C-terminal domain of β_E. (B) The structure of the β_{DP} subunit of the model ATP waiting state compared to X-ray structures: the model ATP waiting structure (light orange), the catalytic dwell state (gray; PDB ID: 1BMF) (5), and the recent 32° rotated structure of Rees *et al.* (orange; PDB ID: 4ASU) (33). The structures are generated by superimposing all α subunits. The γ subunit is also shown, in which the C-terminal domain of β_{DP} in the catalytic dwell structure (β_{DP} of the transparent gray structure) clashes with the γ subunits of the model ATP waiting structure (transparent light purple) and the recent Rees *et al.* structure (purple), causing the rotation of the γ subunit. (C) The average RMSDs (and errors) of the simulated β_{DP} subunit relative to various β conformations. For each β_{DP} structure

saved during the all-atom explicit water MD simulations, the RMSD is computed relative to each reference X-ray structure: PDB ID for β_{DP} and β_E is 1E1R, for β_{HO} is 2HLD_I (the first F_1-ATPase complex among three F_1-ATPase complexes found in the crystallographic asymmetric unit), and for β_{HC} is 1H8E. The γ rotation angle of the catalytic dwell state is 200° and of the model ATP waiting dwell is 240°. For 200° simulations, the pre-hydrolysis state has ATP in β_{DP} and P_i in β_E, the post-hydrolysis state has ADP and P_i in β_{DP} and P_i in β_E, and the post-release state has ADP and P_i in β_{DP} and β_E is empty. (D) Normalized histogram of B^C angles of β_{DP} and β_E subunits for each MD simulation. Similar to (C), ATP; P_i represents the pre-hydrolysis state, ADP+P_i; P_i represents the post-hydrolysis state, and ADP+P_i represents the post-release state for the 200° simulations. The B^C angle distributions of β_{DP} and β_E for the ATP waiting dwell simulation at 240° are significantly different from the catalytic dwell state simulations. (E) Structural change of the C-terminal domain of the α subunits after ATP hydrolysis and P_i release. The structures are obtained by averaging the configurations saved during the all-atom explicit water MD simulation, and by overlaying the $\alpha_3\beta_3$ crown part of the structure with the starting structure (i.e. the energy minimized Walker structure). For clarity, only the α and γ subunits are shown: α_{TP} (red), α_{DP} (light green), and α_E (blue) for the post-release state. The structure of the pre-hydrolysis state is shown in gray.

Figure S3. (A) Simulations of an isolated β subunit in explicit solvent with various nucleotide occupancies (see Methods), starting from the closed β_{DP} conformation in the Bowler *et al.* structure (PDB ID: 2JDI) (20). The equilibrium averages of the B^C helical crossing angle for 12 independent simulations, each 20 ns, are plotted. (B) The potential of mean force (PMF) along the B^C angle (abscissa) and a β-sheet twisting angle

(ordinate) in degrees (see *SI Appendix*, SI6). The occupations are (a) Mg+ATP, (b) Mg+ADP+P_i, (c) MgADP, (d) MgP_i, and (e) empty. The sampling was initiated from the $\beta_{DP}\rightarrow\beta_E$ TMD transition pathway. The positions of crystallographic β-conformations are marked on (a): '+' for β_{DP} and β_{TP}, 'o' for the partly open β_{DP} at 240° found in the simulations, '*' for β_{HC}, '—' for β_E.

Figure S4. P_i release pathways: backdoor I (red), backdoor II (green), and front door (blue). (A) The β_E subunit is represented by the yellow surface, and the α_E subunit is not shown to make the release pathways visible. Other α and β subunits are shown in dark gray, the γ subunit in pink, and the P-loop is shown in purple. (B) Blow-up of (A): β_E is represented by yellow-cartoon and the P-loop by purple cartoon. ADP is shown in stick-representation directly below the front door. Each P_i release pathway is represented by a color-coded mesh. For clarity, the γ and other α and β subunits are omitted. (C) Comparison of P_i release probabilities through the main release pathways to the overall release probabilities. The main release pathway is via backdoor II from the β_{DP} with ADP, P_i, and Mg^{2+} at 240° (black dotted line), and the front door from β_{DP} with P_i at 240° (red dotted line) and from β_E with P_i at 200° (blue dotted line), respectively. For each case, the corresponding P_i release probability through all pathways is presented by a solid line.

Figure S5. P_i and ADP release probabilities from β_{DP} at 200° and 240°, respectively. For each case, the P_i release probability through the front door is also presented in the dotted line. The MCES simulations were carried out by reproducing the ADP and P_i (see Methods); see also *SI Appendix*, Fig. S4.

Figure S6. Comparison of the C-terminal domain orientation of the β_E subunits: X-ray crystal structure (PDB ID: 1E1R (34); light gray), average structure from the all-atom explicit water MD simulation of the 240° ATP waiting state model (light orange), and the 240° γ rotated structure generated from the $\gamma+\beta_{DP}$ TMD simulations (yellow). For comparison, the γ subunit is also shown: light gray for the X-ray structure (1E1R) and purple for the 240° ATP waiting state model structure. The MD averaged structure is are obtained by averaging the configurations saved during the all-atom explicit water MD simulation, and by overlaying the $\alpha_3\beta_3$ crown part of the structure to the starting structure (i.e. the energy minimized crystal structure). The comparison shows that the β_E subunit generated from the TMD simulation is slightly more closed than that of the 240° ATP waiting state model average MD structure, which in turn is slightly more closed than the 200° X-ray structure. In the right panel, we show the β_E/γ catch interaction for the 200° state (1E1R; β_E and γ: light gray) and the partial breakage of the catch interaction in the 240° ATP waiting state model ($\gamma+\beta_{DP}$ TMD simulation; β_E: yellow; γ: purple), which occurs as the γ subunit rotates counter clockwisely relative to β_E viewed from the membrane.

Figure S7. (A) The rotation of the C-terminal domain of α_{DP} (light green) toward β_{DP} (orange) after the hydrolysis of ATP. For comparison, the structure of the pre-hydrolysis state is shown in gray. Within the box, the interaction between α_{DP}R373 (purple stick representation) and the P_i cleaved from ATP (yellow stick representation) is shown. For comparison, the position of α_{DP}R373 in the pre-hydrolysis state is shown in gray stick representation. Each structure is obtained by averaging the configurations saved during the all-atom explicit water MD simulations. (B) Comparison of the dimeric interface

between the α_{DP} and β_{DP} subunits of X-ray structures: AMPPNP (PDB ID: 2HLD_I (3); β_{DP} and α_{DP}: light-gray), transition-state mimic (1E1R; β_{DP}: gold; α_{DP}: palegreen), and ADP bound complexes (1BMF; β_{DP}: orange; α_{DP}: green). The α_{DP}/β_{DP} interface is compared between 1E1R and 2HLD_I structures in the left panel and between 1BMF and 2HLD_I structures in the right panel, respectively. The figure shows that between the two sets of structures, there is a rearrangement of the C-terminal domain of α_{DP} toward β_{DP}. In the left panel, the circled region shows an enlarged view after a slight rotation for a clear presentation of the interaction between α_{DP}R373 (2HLD_I shown in gray and 1E1R in palegreen) and an ATP-analog and the transition-state mimic. (C) Several interactions that are found at the interface between α_{DP} toward β_{DP} of 1E1R (transition-state mimic; β_{DP}: gold; α_{DP}: palegreen) and 2HLD_I (AMPPNP; β_{DP} and α_{DP}: light-gray). (D) Comparison of α_E/β_E subunits of P_i/SO_4^{2-} bound X-ray structures (PDB ID: 2HLD_II (the second complex in the asymmetric unit of 2HLD; β_E: light green; α_E: light blue) and 1E79 (35) (β_E: light yellow; α_E: slate)) to the β_E-empty X-ray structure (1BMF; both shown in gray cartoon). In the left panel, the pair 2HLD_II and 1BMF and in the right panel, the pair 1E79 and 1BMF are shown, respectively. The C-terminal domain of α_E of the β_E-empty complex is rotated slightly away from that of P_i/SO_4^{2-} bound complex. (E) The packing of α_E (blue) against β_{DP} (orange). The structure is viewed from the membrane. Also shown is the coiled coil region of the γ subunit (gray) that has surface contacts with the α_E and β_{DP} subunits.

Figure S8. Cross-correlation maps: (A) pre-hydrolysis state, (B) post-hydrolysis state, and (C) post-release state, respectively. The diagonal blocks are for the intra-subunit cross-correlation for each subunit, and the off-diagonal blocks are for the inter-subunit

cross-correlations. The color scale changes between red for 1.0 (positive correlation) and blue for -1.0 (anti-correlation), and white is for 0.0 (no-correlation). In (D), the cross-correlation map between α_E and β_E for the post-release state is shown with annotation of each structural element in the β subunit: NTD (N-terminal domain), NBD (nucleotide binding domain), CTD (C-terminal domain), P-loop, and helix H, respectively.

Figure S9. The buried surface area and standard error ($Å^2$) between two neighboring subunits: top for the pre-hydrolysis state (ATP/P_i), middle for the post-hydrolysis state (ADP+P_i/P_i), and bottom for the post-release state (ADP+P_i), respectively. For each pair of subunits, the buried surface area is defined as a half of the sum of the solvent accessible surface area of each subunit minus the total solvent accessible surface area of the two subunits. In the computation of the buried surface area, we consider only given two subunits, and any contribution from neighboring subunit are ignored with an assumption that those subunits do not interfere the interface formed between the two given subunits. The thickness of the zigzaged lines and arrows are scaled according to the relative magnitude of the buried surface area.

Figure S10. Comparison of the β_E subunit structures from various X-ray structures with or without P_i in the binding pocket. In (A), β_E subunit structures with P_i (or P_i analog) are overlaid to β_E subunit structures with empty binding pocket. For β_E subunit with empty binding pocket, the structures are represented by the pale-yellow cartoon (PDB-ID: 1BMF and 2HLD_I); for β_E subunit with P_i (or sulfate), the structures are represented by the red cartoon (PDB-ID: 1E1R, 1E79, and 2HLD_II), respectively. The figure presents that all β_E subunit structures are essentially identical independent of the presence of bound P_i (or P_i-analog) in it. The two sets of β_E structures are superimposed each other

by using the C_α atoms. The colors of the two P_i molecules are blue (binds in the P-loop) and green (binds in the second binding site), respectively. The α_E subunit is shown by the dark gray cartoon and the γ subunit by the light gray cartoon, respectively. (B) Blow-up around the binding pocket. The residues that interact with P_i are shown in the stick-representation: β_ER189, β_EN257, and the residues in the P-loop. The residues in pale-yellow are for the structure with an empty binding pocket (1BMF), and the residues in red are for the structure with P_i in the binding pocket (1E1R).

Figure S11. The γ-rotation angles from the TMD simulations: (red) all β+α simulation of no-P_i system; (yellow) all β+α simulation with P_i in β_E; (blue) all β+α simulation with P_i in β_E and with no interaction between P_i and α_ER373. The simulation time is shown in nanosecond, and the γ rotation angle is defined as in Pu and Karplus (6). The simulations are carried out for 1 ns with the TMD perturbations applied to $\alpha_3\beta_3$ component of the system followed by an 1ns unperturbed MD simulations to relax the system, during which each system reached a plateau for rotation angle of γ.

Figure S12. Crystal structures of β_{DP} and β_{TP} with bound ligands. (A) For β_{DP} subunit with ADP and azide (PDB-ID: 2CK3), the structure is represented by the gold cartoon, ADP and the side chains in the P-loop, β_{DP}R189, β_{DP}N257, and β_{DP}R260 by a stick representation, and the azide ion by a sphere. (B) For the β_{TP} (PDB-ID: 2HLD_I) subunit, the protein is represented by light green cartoon, AMPPNP and the side chains in the P-loop, β_{TP}R189, β_{TP}N257, and β_{TP}R260 by a stick representation.

Figure S13. Proposed disulfide cross-linking sites between β_{TP} and γ subunits: 240° β_{TP} (brown), 240° γ (purple), and 200° β_{TP} and γ (gray). The residues involved in the

proposed disulfide cross-linking residues ($\beta_{(TP)}$D394/γG76 and $\beta_{(TP)}$E398/γS114) are shown in stick representation.

Figure S1

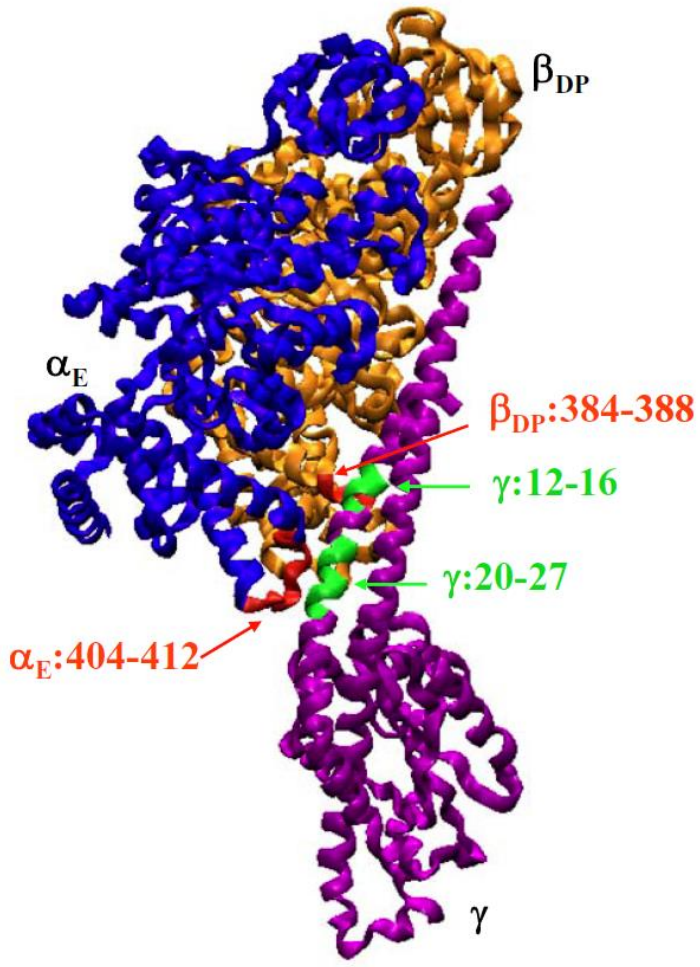

Figure S2

A)

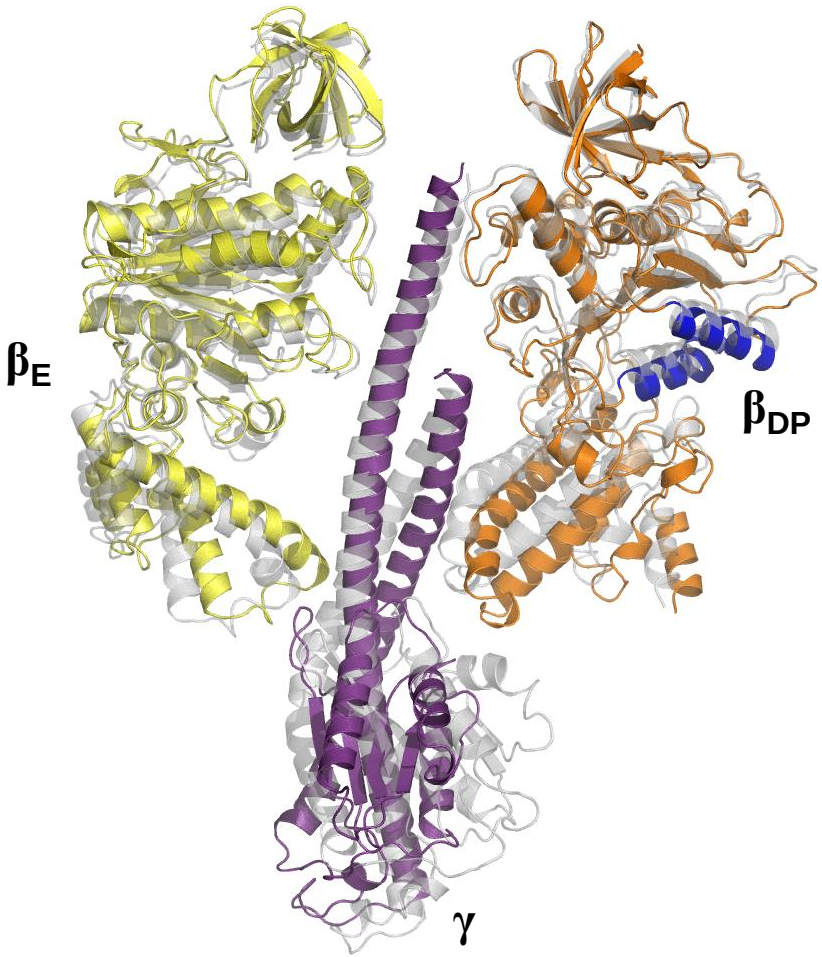

Figure S2

B)

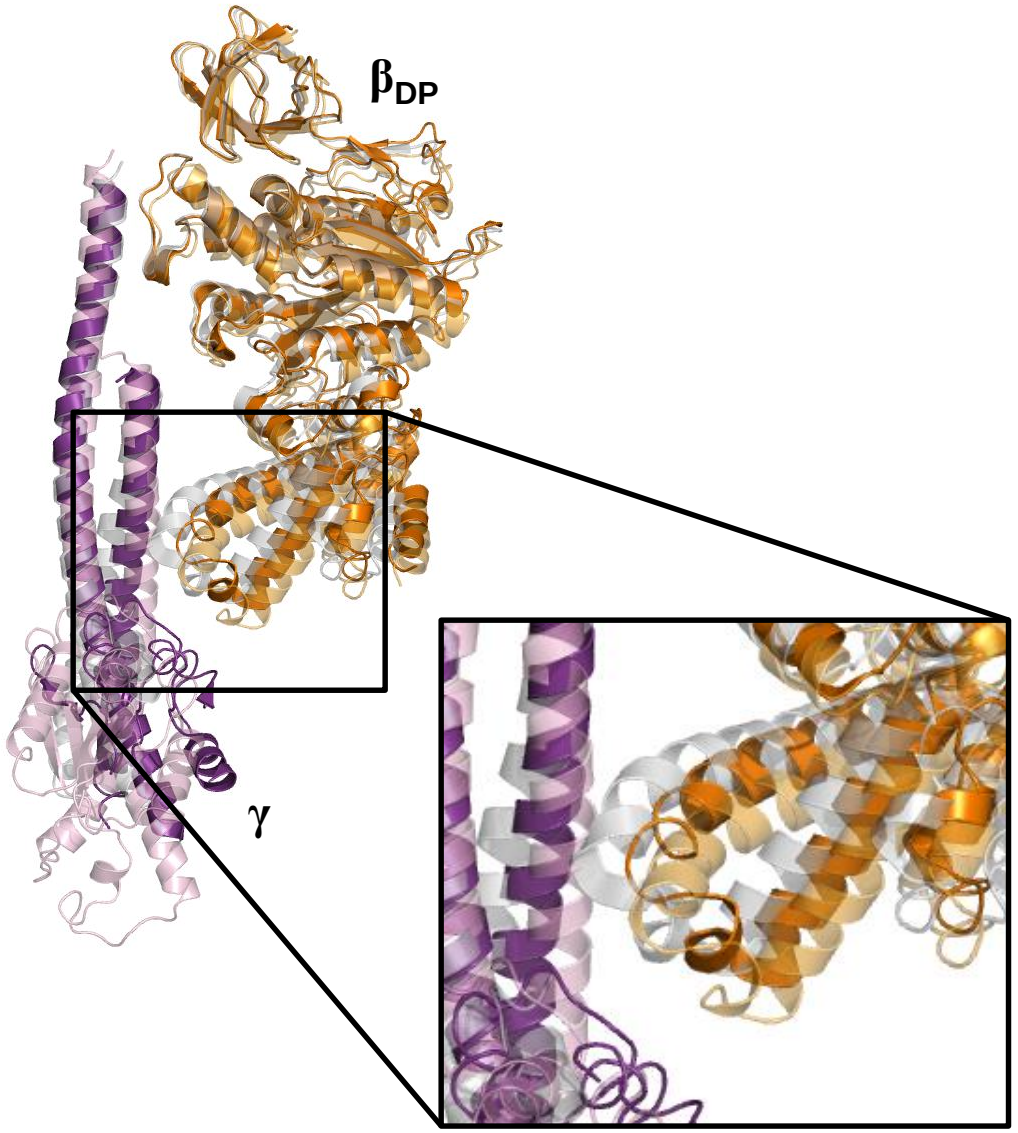

Figure S2

C)

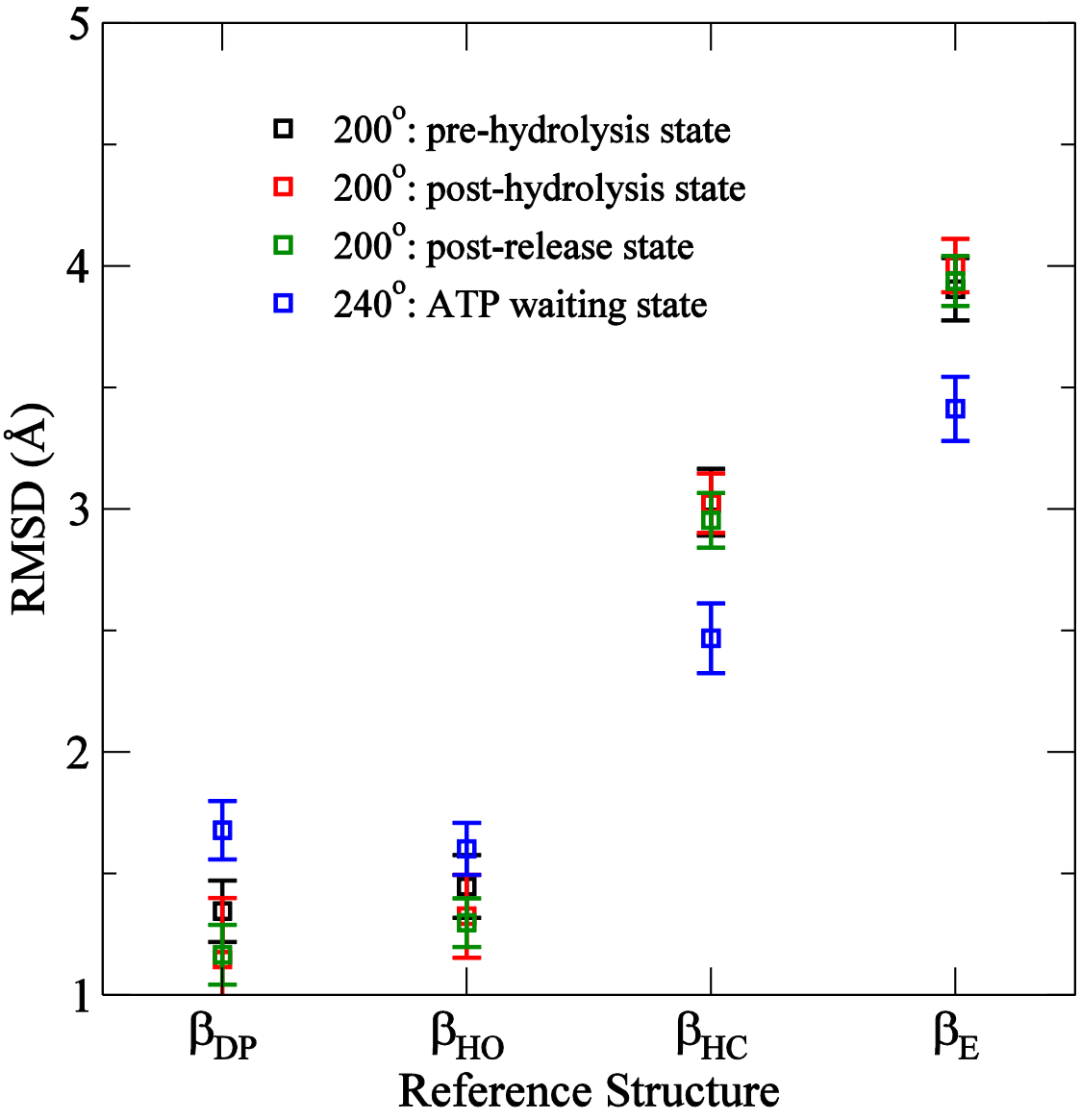
200°: pre-hydrolysis state
200°: post-hydrolysis state
200°: post-release state
240°: ATP waiting state
RMSD (Å)
5
4
3
2
1
βDP
βHO
βHC
βE
Reference Structure

Figure S2

D)

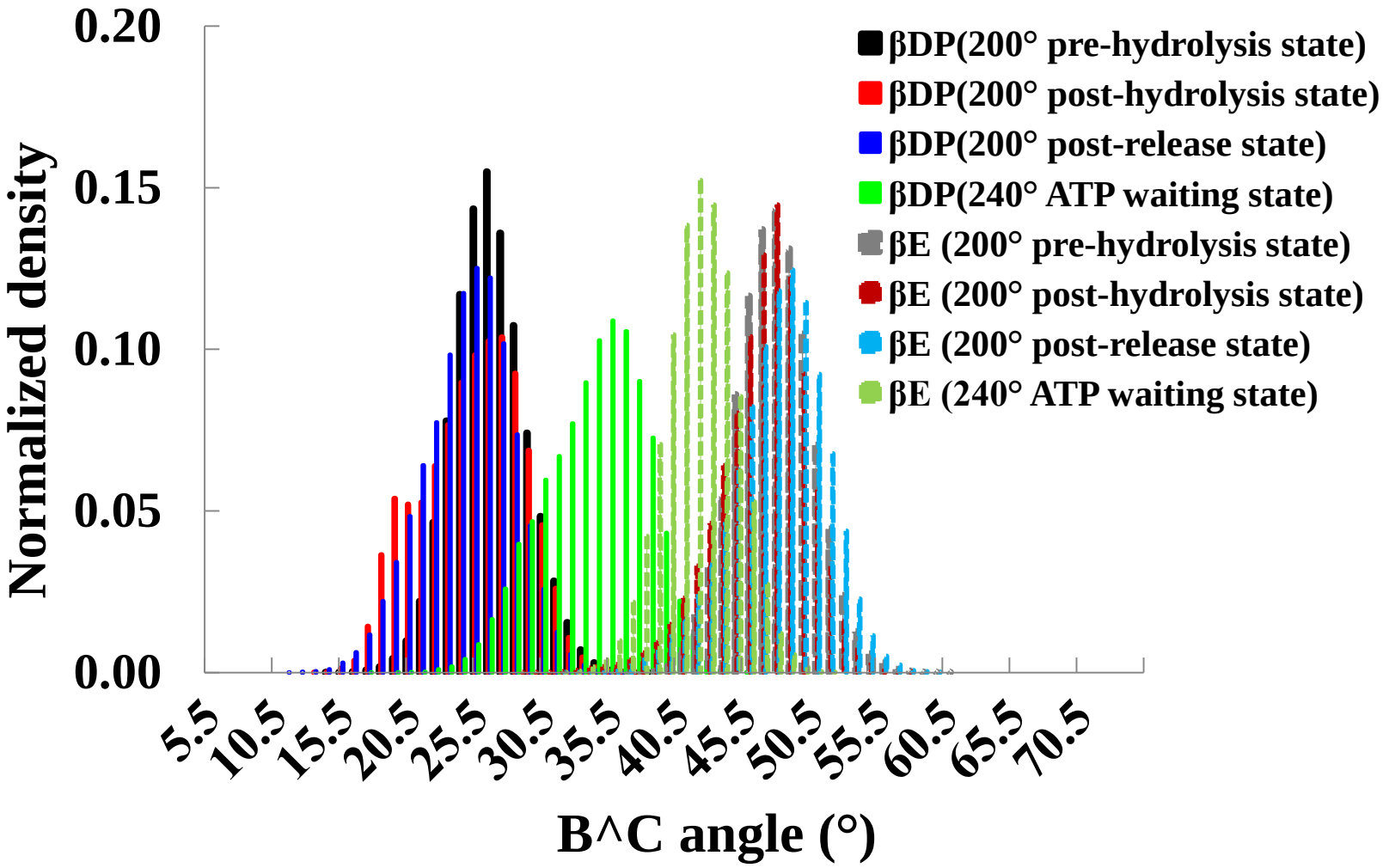
0.20
0.15
0.10
0.05
0.00
Normalized density
5.5
10.5
15.5
20.5
25.5
30.5
35.5
40.5
45.5
50.5
55.5
60.5
65.5
70.5
B^C angle (°)
βDP(200° pre-hydrolysis state)
βDP(200° post-hydrolysis state)
βDP(200° post-release state)
βDP(240° ATP waiting state)
βE (200° pre-hydrolysis state)
βE (200° post-hydrolysis state)
βE (200° post-release state)
βE (240° ATP waiting state)

Figure S2

E)

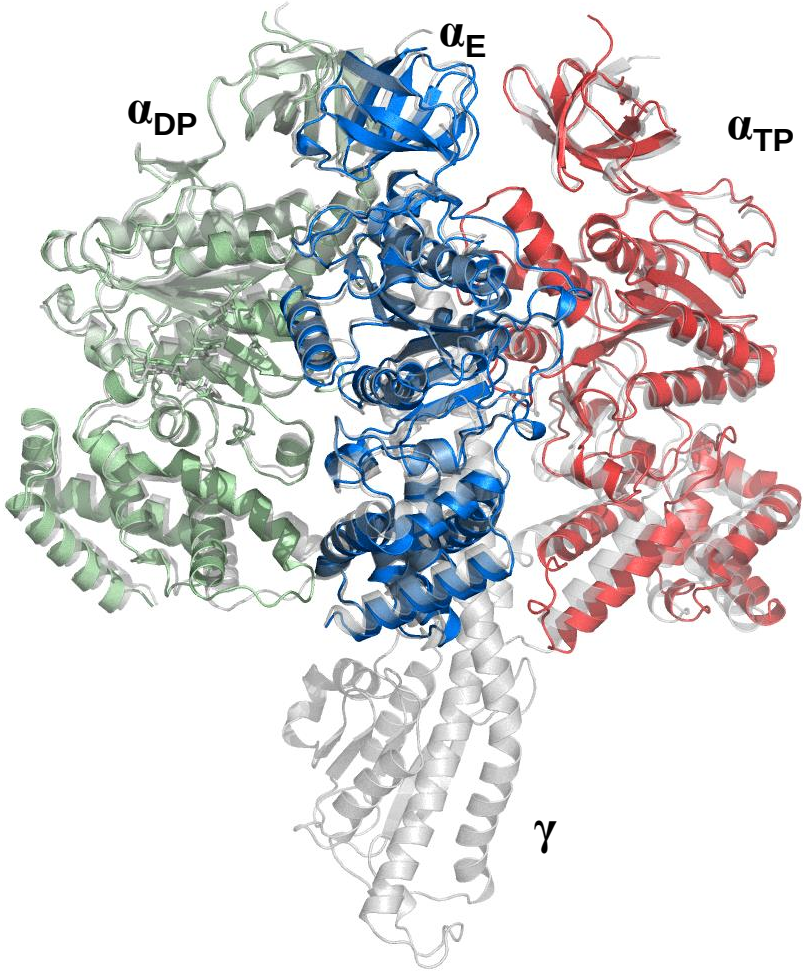

Figure S3

A)

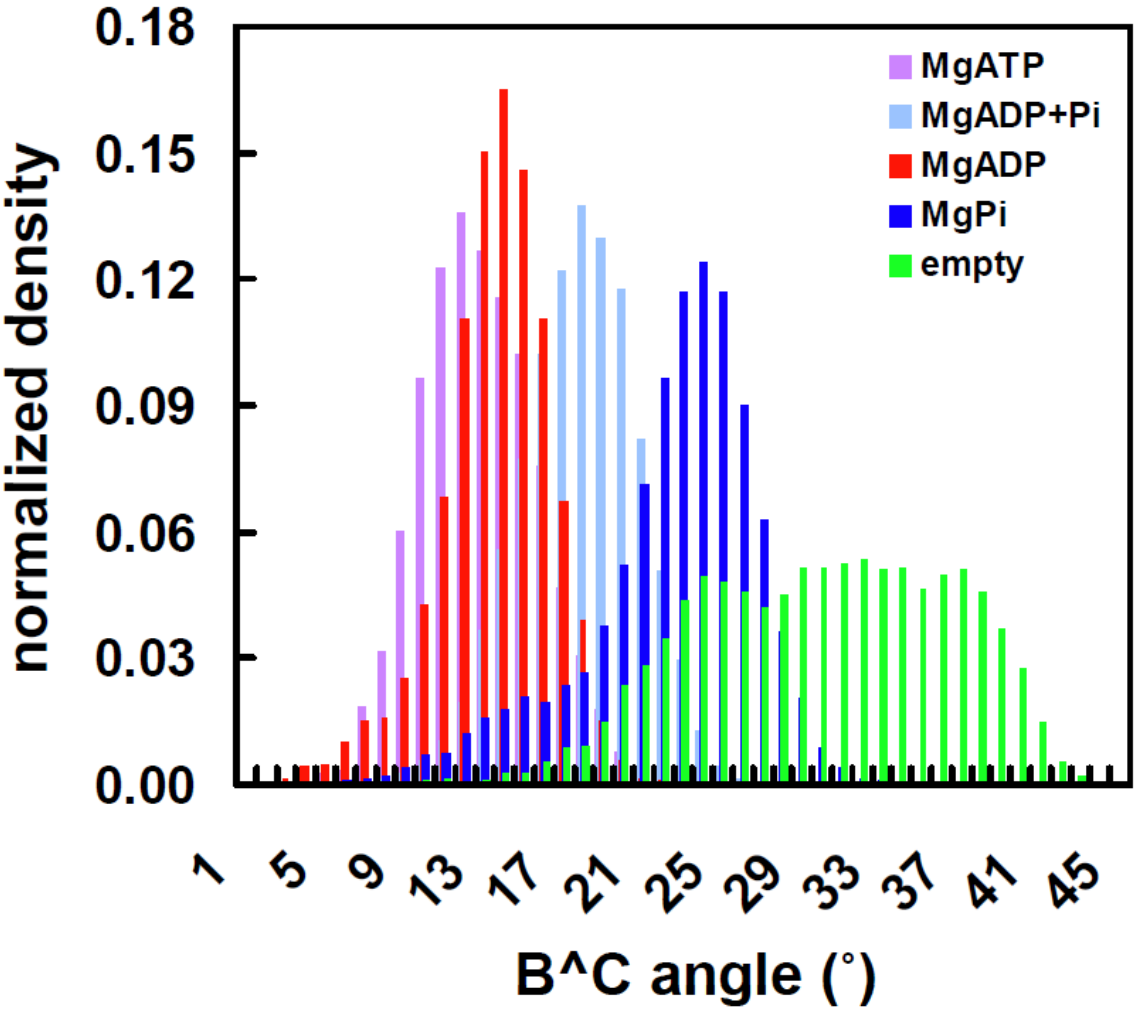
0.18
0.15
0.12
0.09
0.06
0.03
0.00
normalized density
MgATP
MgADP+Pi
MgADP
MgPi
empty
1
5
9
13
17
21
25
29
33
37
41
45
B^C angle (°)

Figure S3

B)

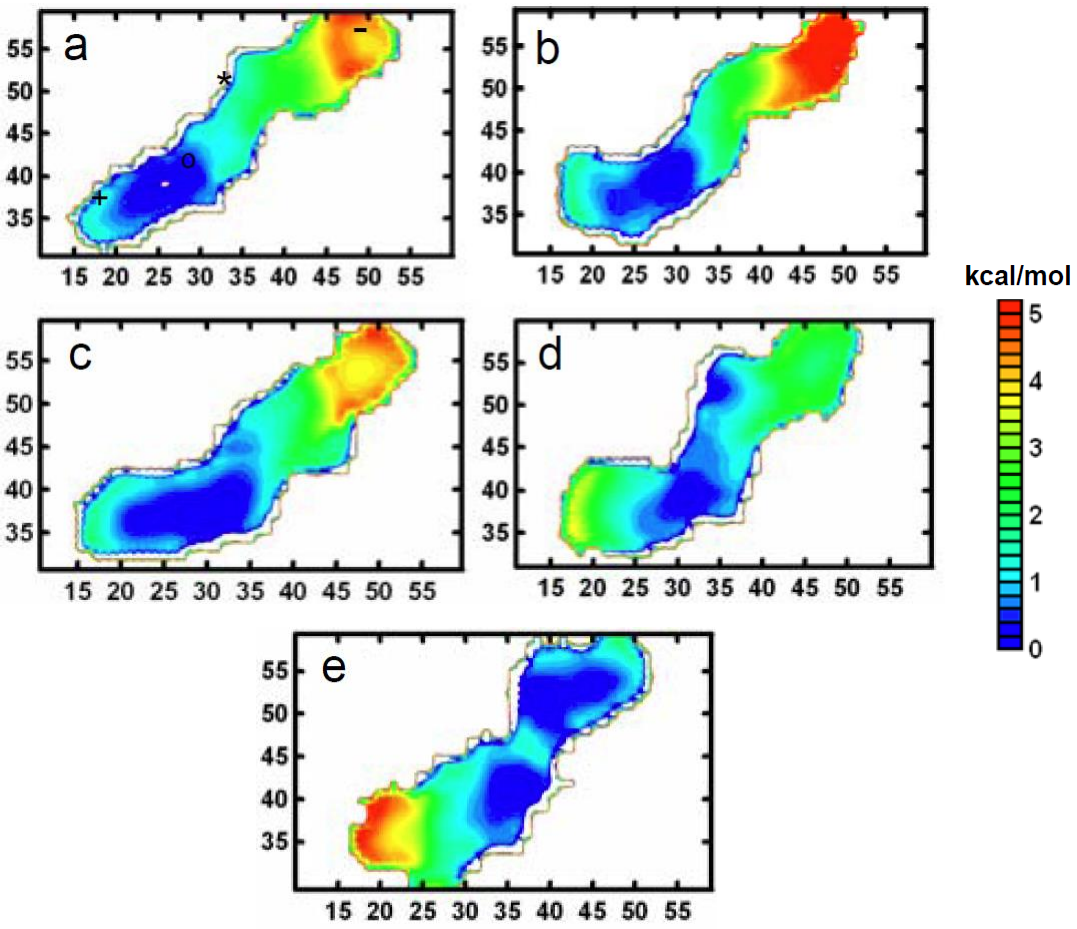

Figure S4

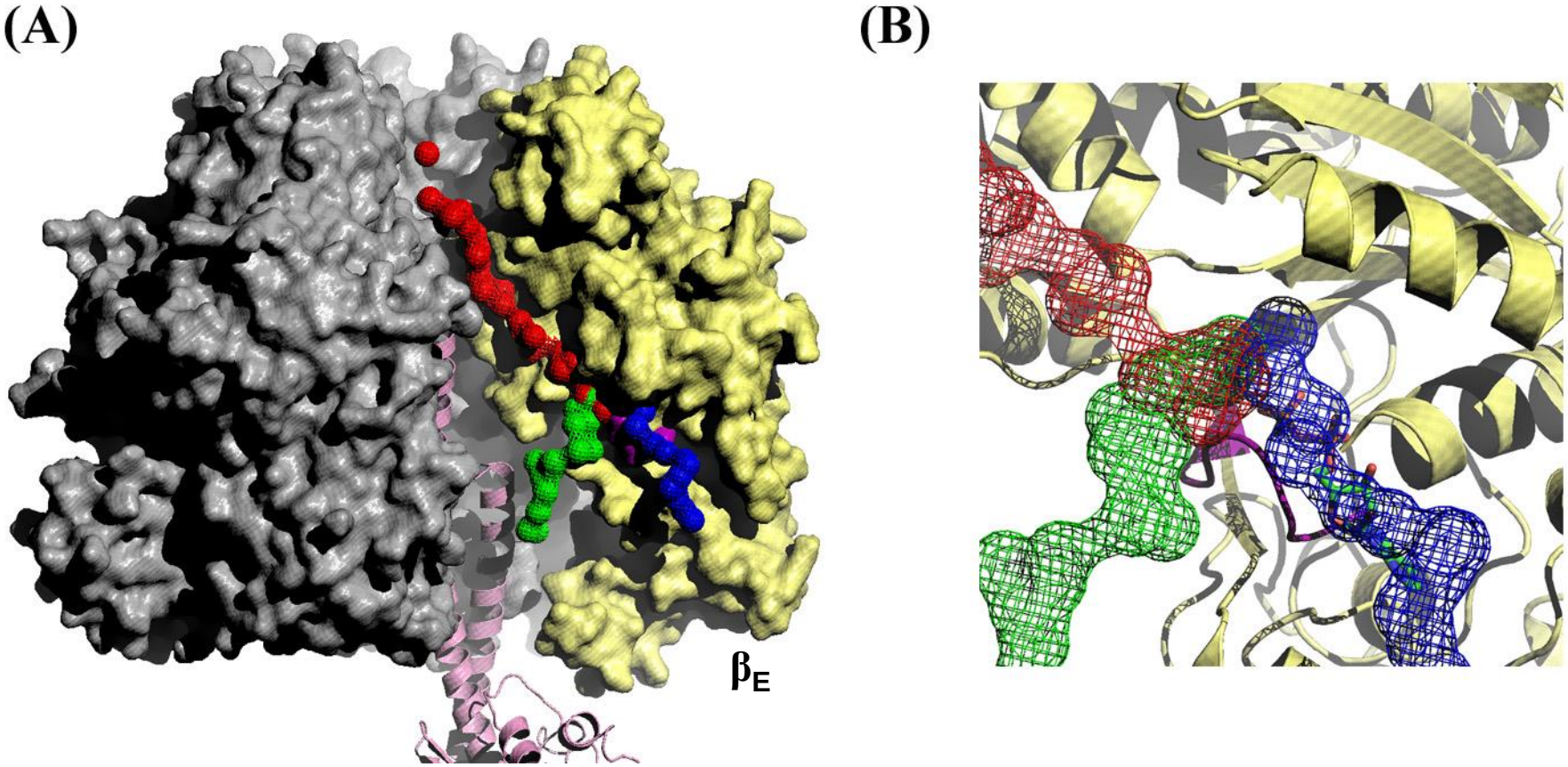

Figure S4

C)

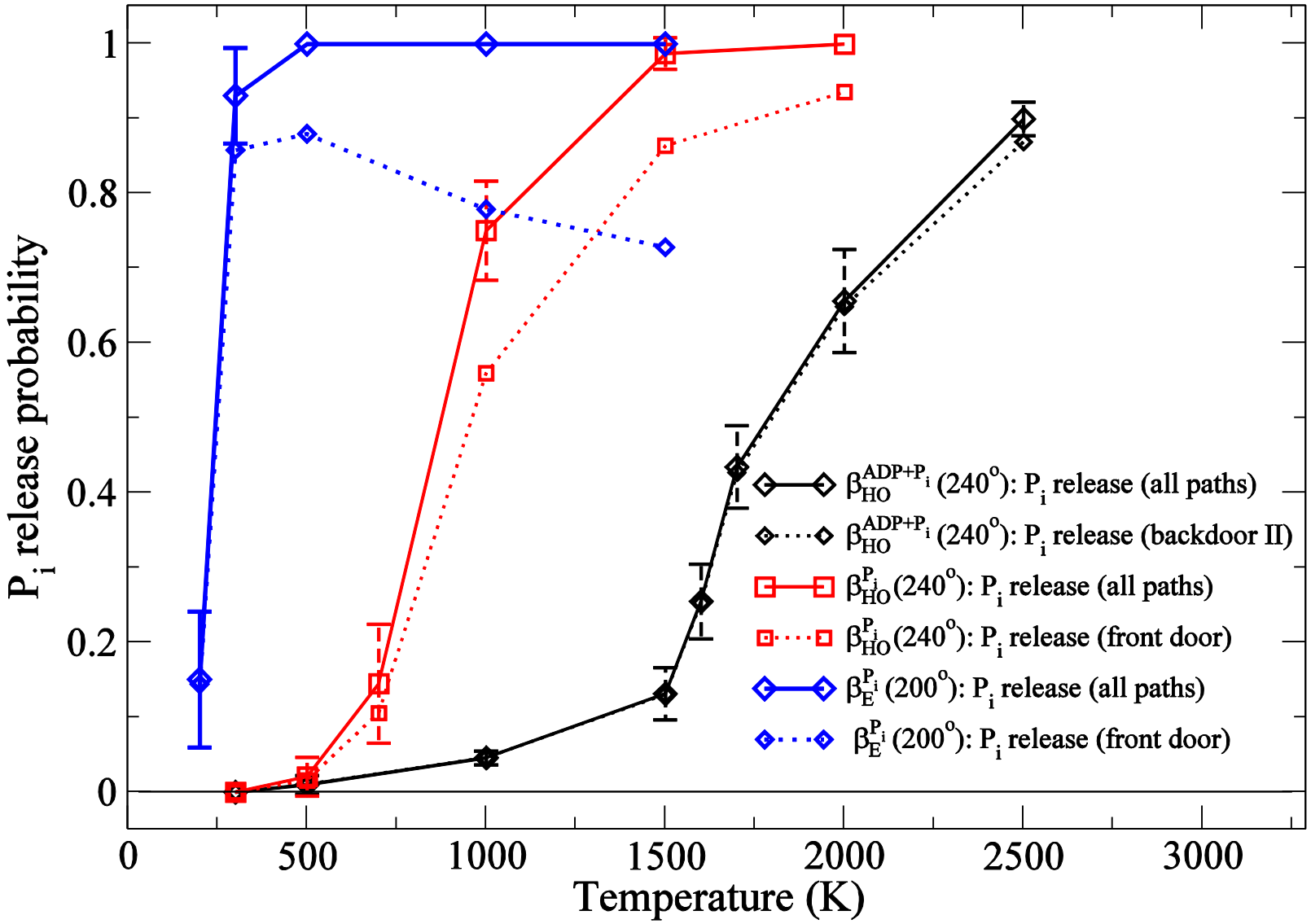
P_i release probability
Temperature (K)
0
0.2
0.4
0.6
0.8
1
0
500
1000
1500
2000
2500
3000
β_HO^ADP+Pi (240°): P_i release (all paths)
β_HO^ADP+Pi (240°): P_i release (backdoor II)
β_HO^Pi (240°): P_i release (all paths)
β_HO^Pi (240°): P_i release (front door)
β_E^Pi (200°): P_i release (all paths)
β_E^Pi (200°): P_i release (front door)

Figure S5

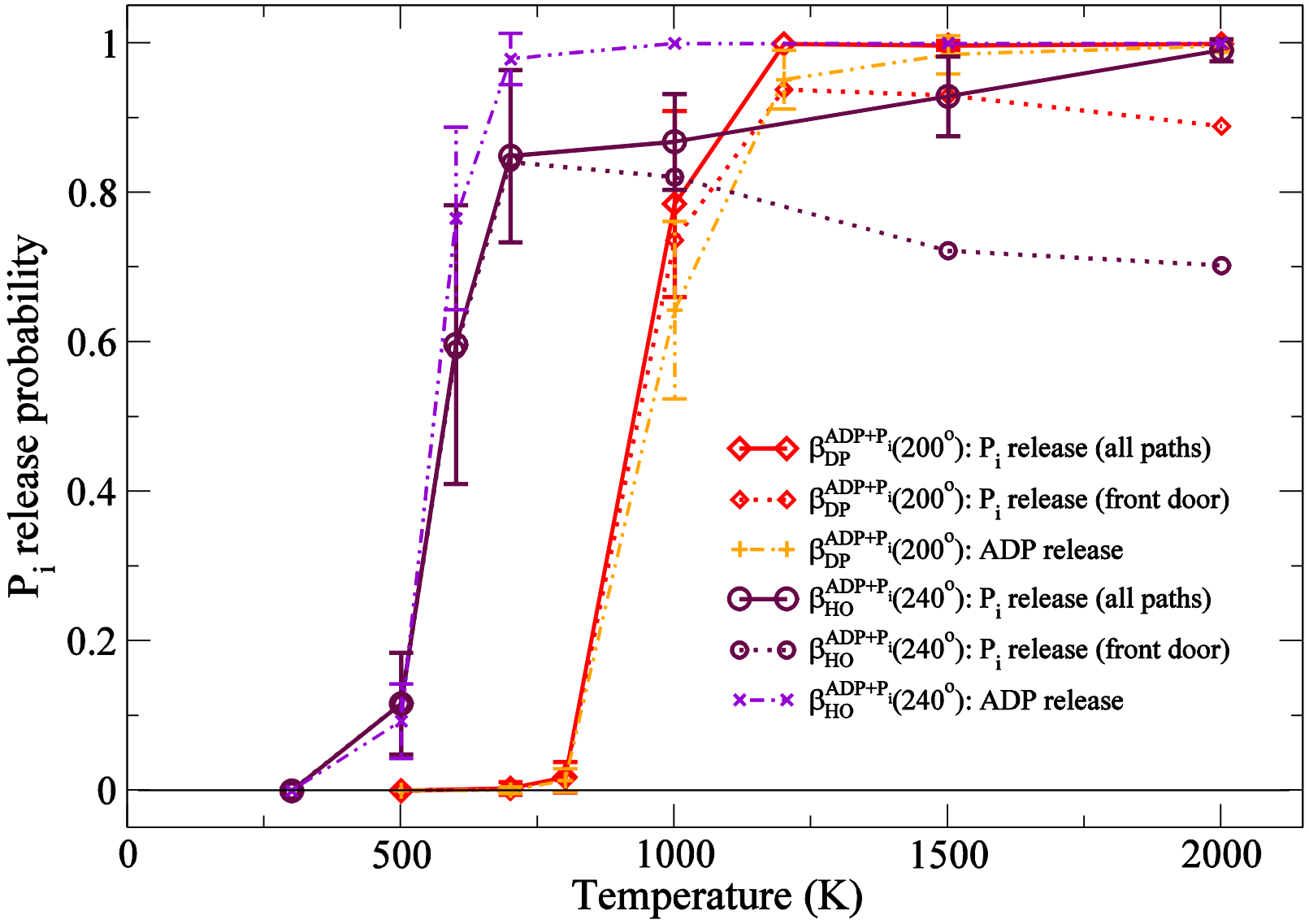
P_i release probability
Temperature (K)
0
0.2
0.4
0.6
0.8
1
0
500
1000
1500
2000
β_DP^ADP+Pi(200°): P_i release (all paths)
β_DP^ADP+Pi(200°): P_i release (front door)
β_DP^ADP+Pi(200°): ADP release
β_HO^ADP+Pi(240°): P_i release (all paths)
β_HO^ADP+Pi(240°): P_i release (front door)
β_HO^ADP+Pi(240°): ADP release

Figure S6

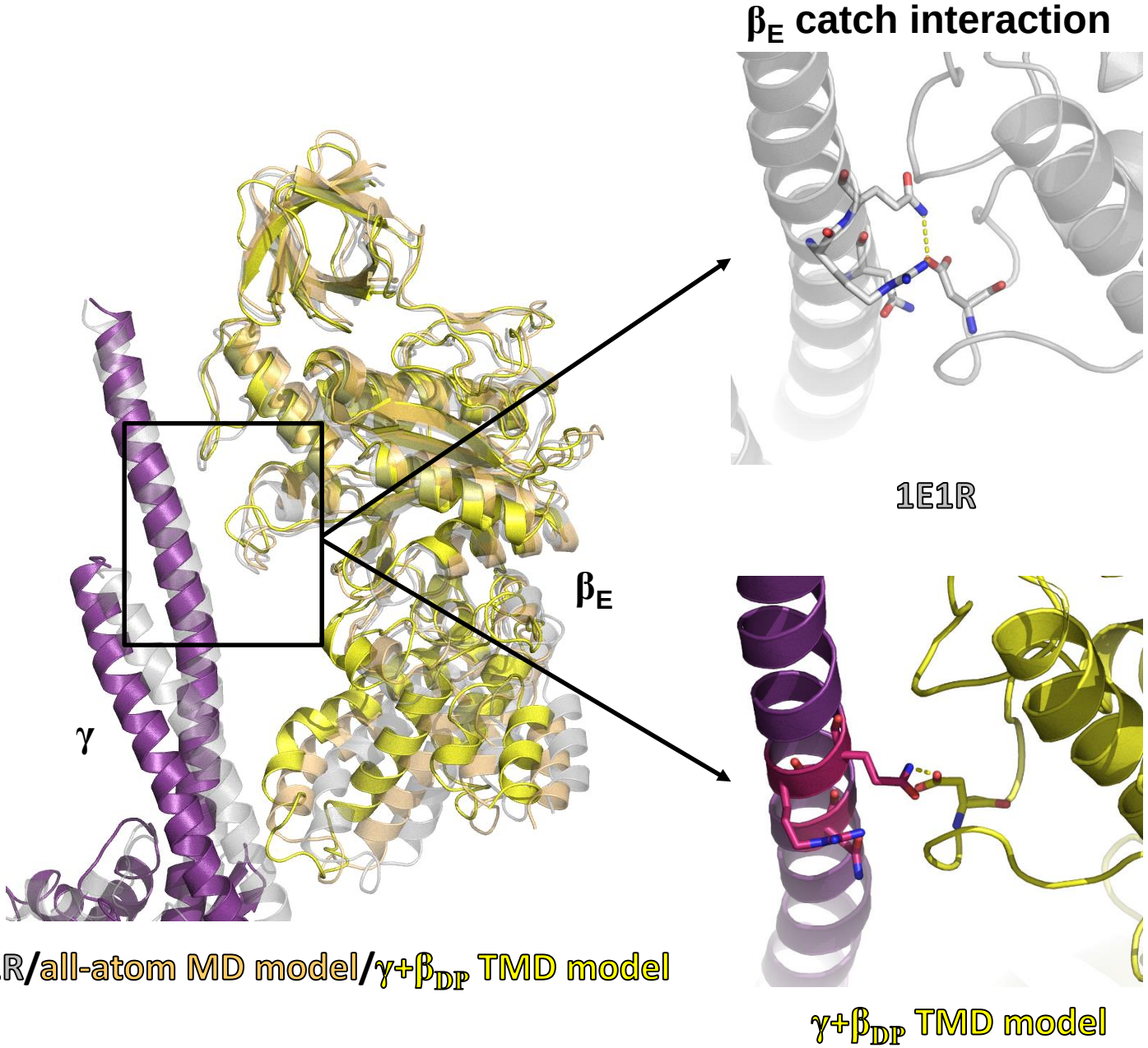
β_E catch interaction
β_E
γ
1E1R
1E1R/all-atom MD model/γ+β_{DP} TMD model
γ+β_{DP} TMD model

Figure S7

A)

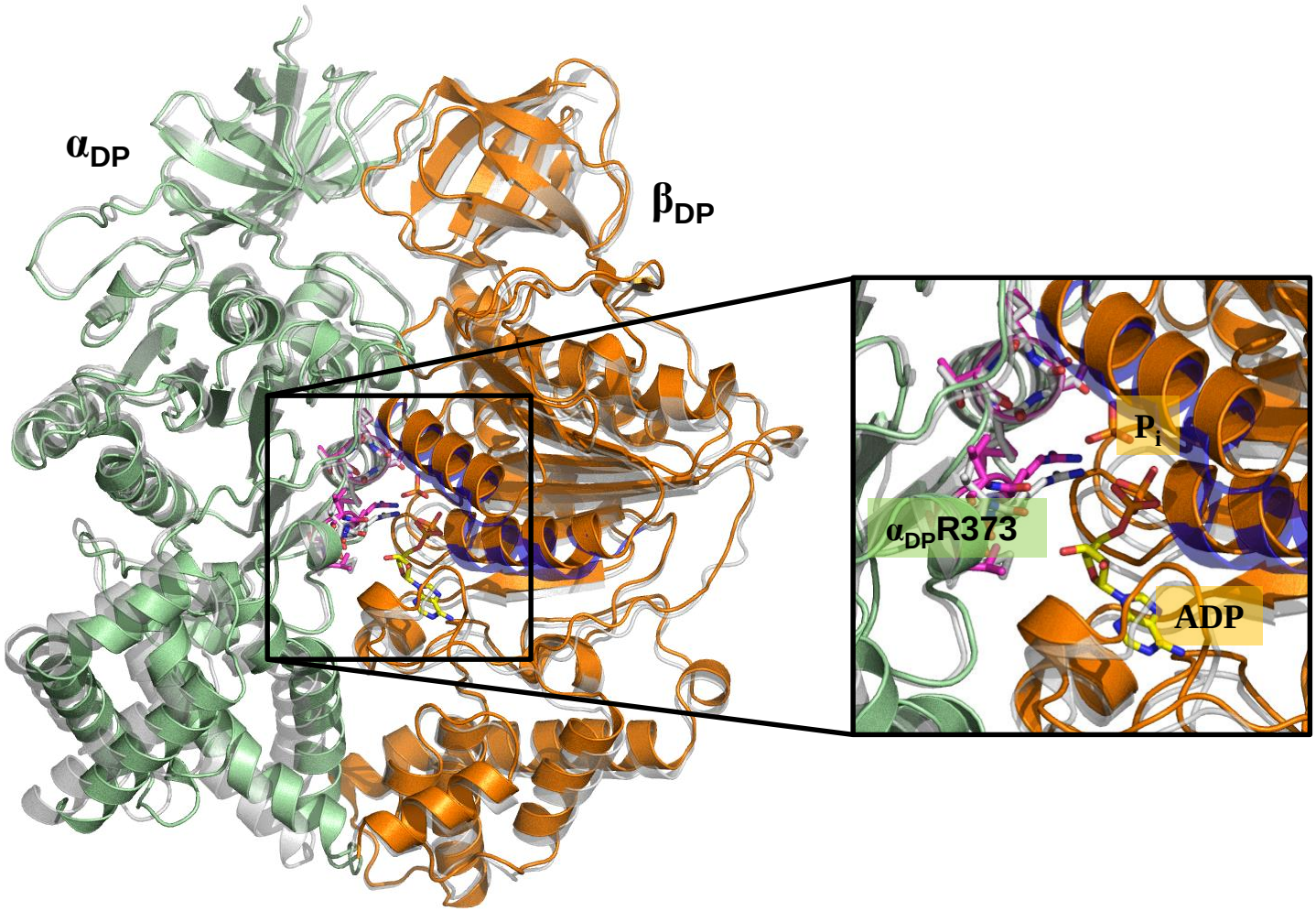

Figure S7

B)

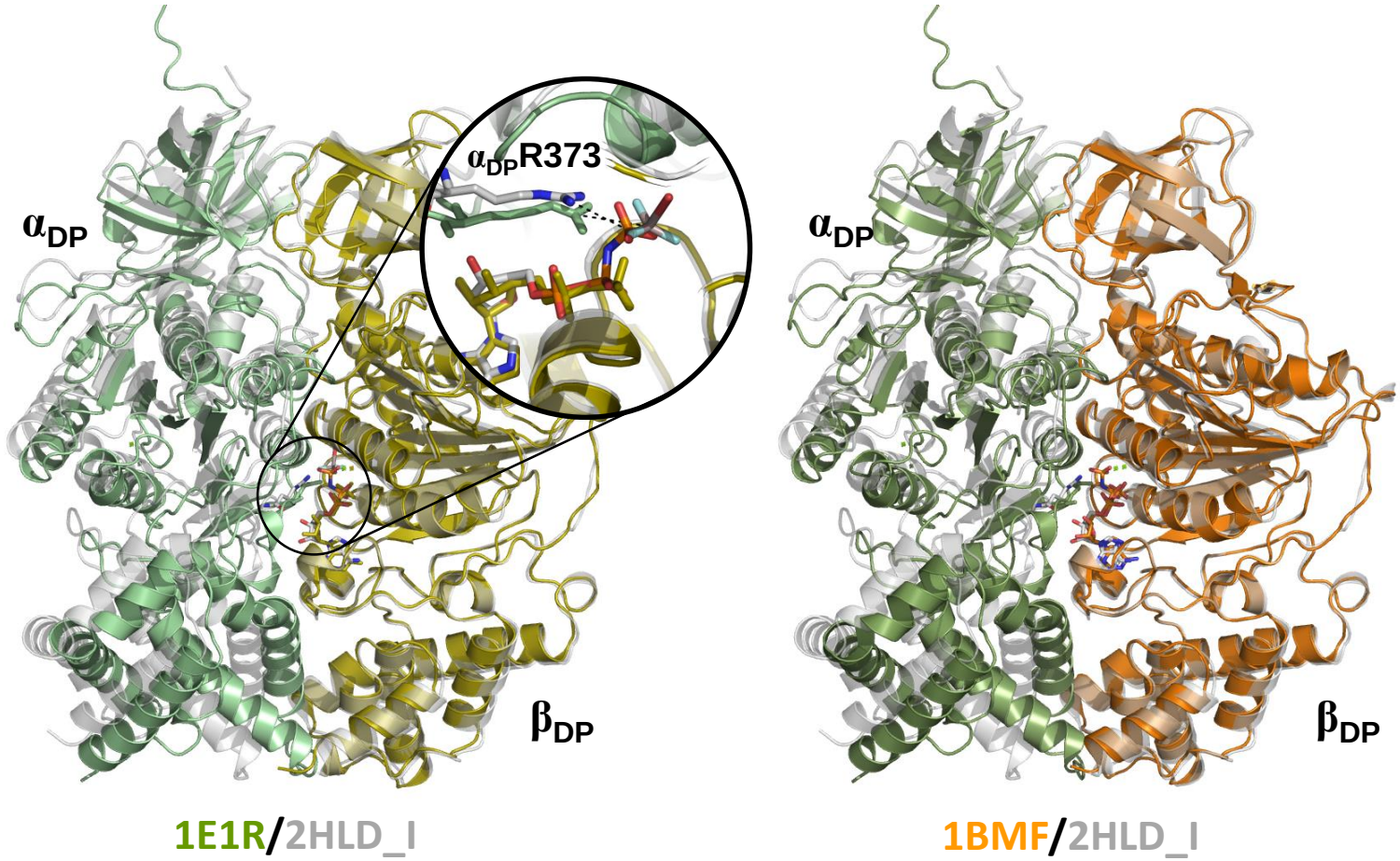

Figure S7

C)

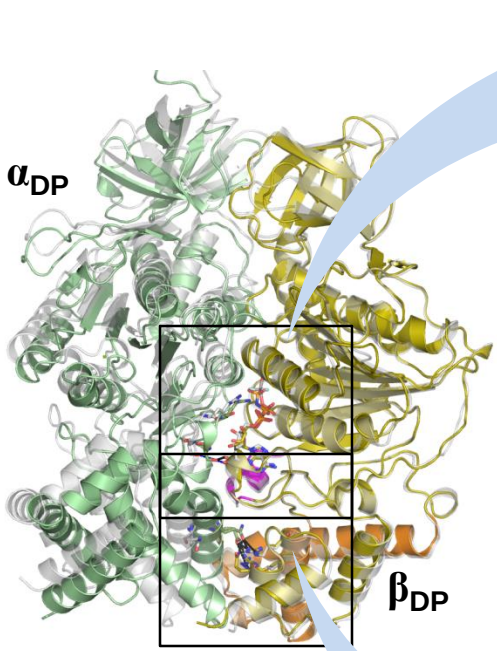
αDP
βDP
1E1R/2HLD

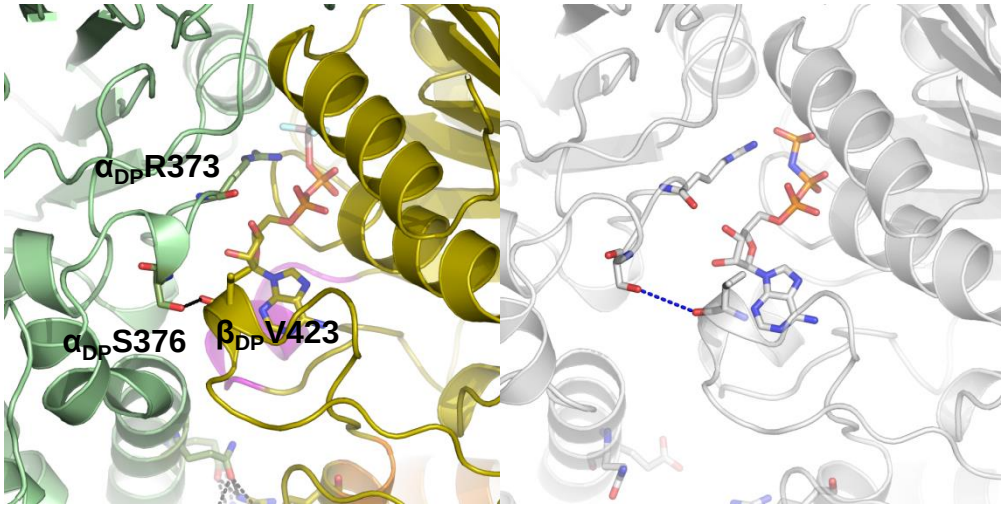
αDPR373
αDPS376
βDPV423
1E1R
2HLD

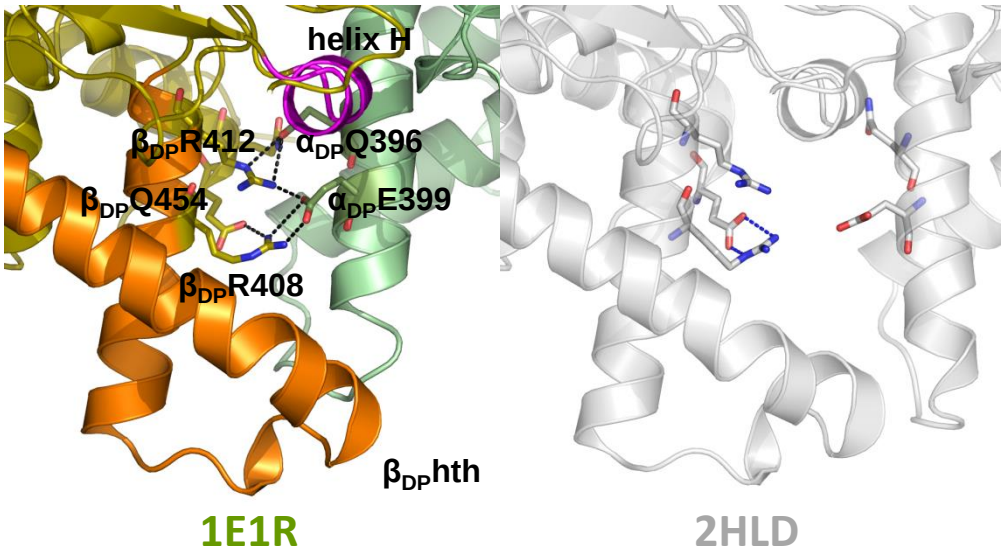
helix H
βDPR412
αDPQ396
βDPQ454
αDPE399
βDPR408
βDPhth
1E1R
2HLD

Figure S7

D)

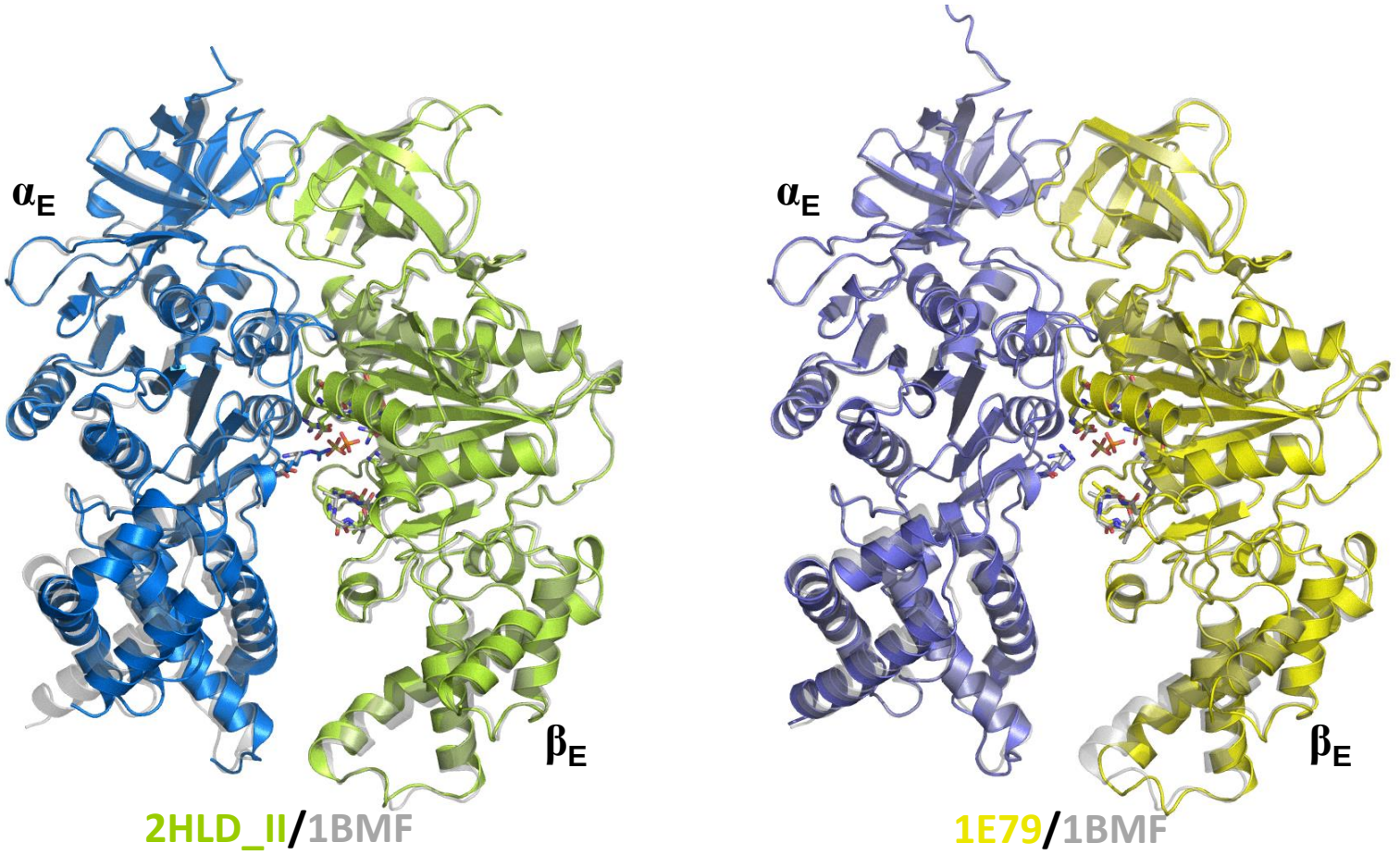

Figure S7

E)

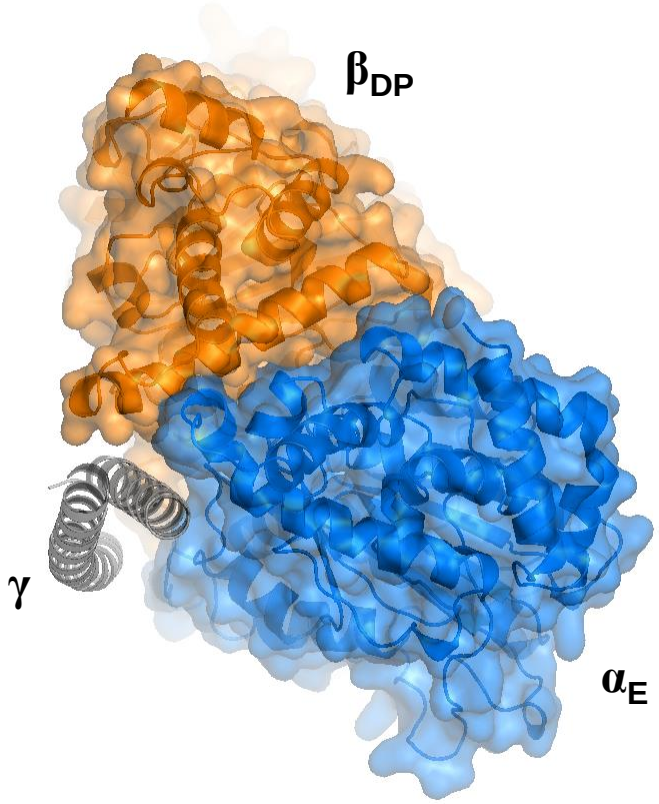

Figure S8

A)

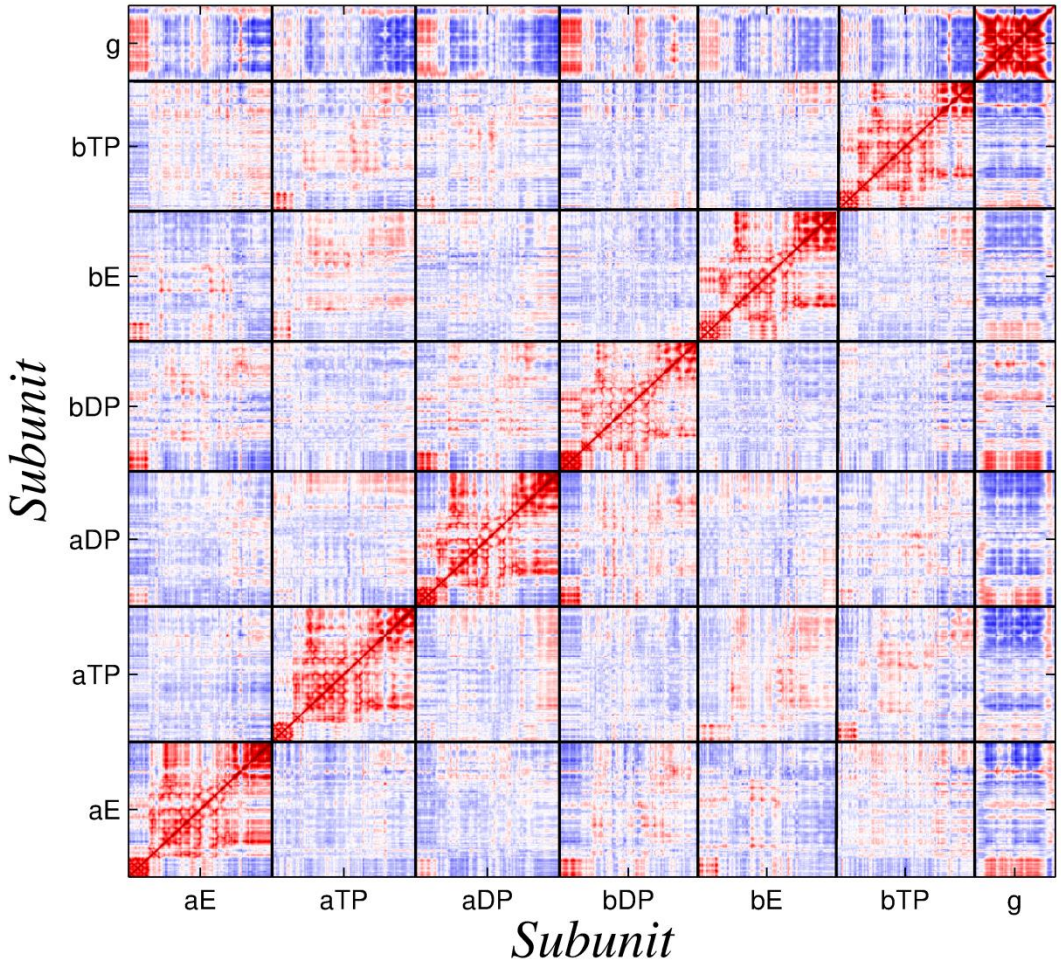

Figure S8

B)

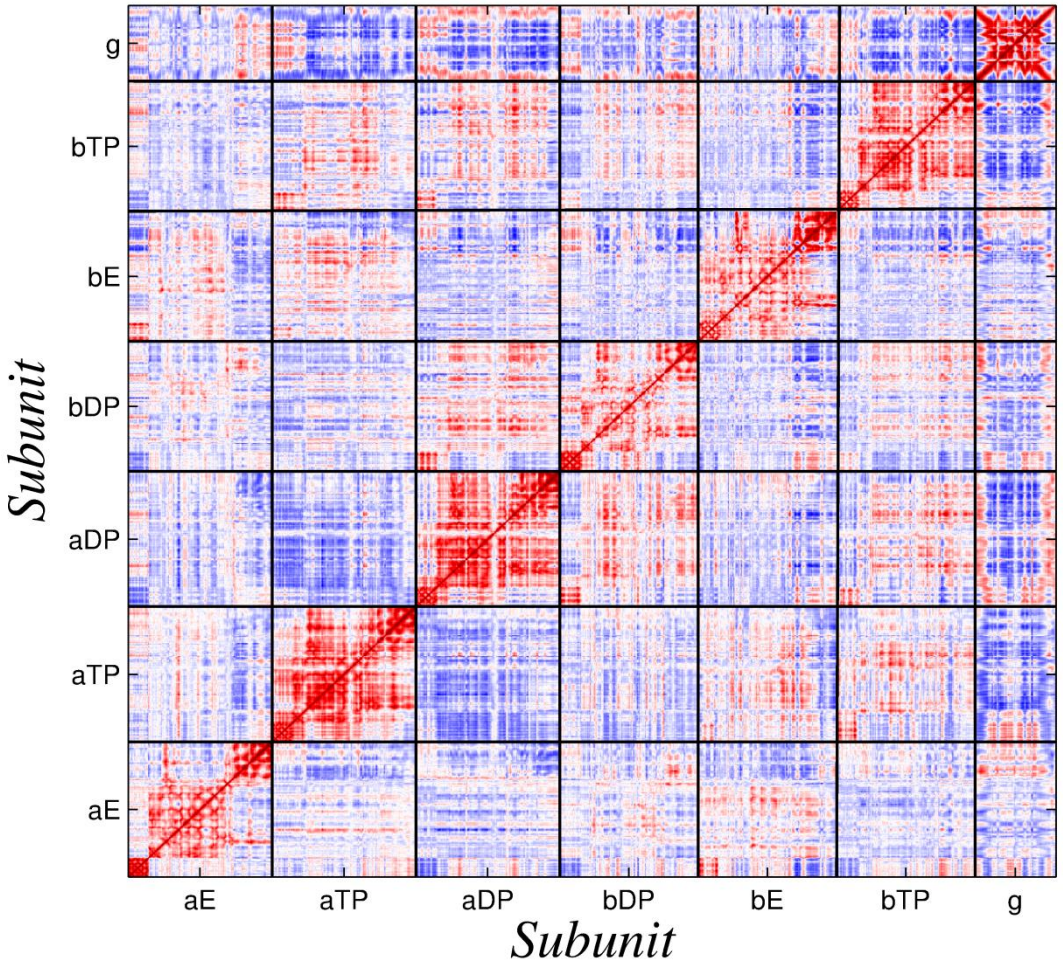

Figure S8

C)

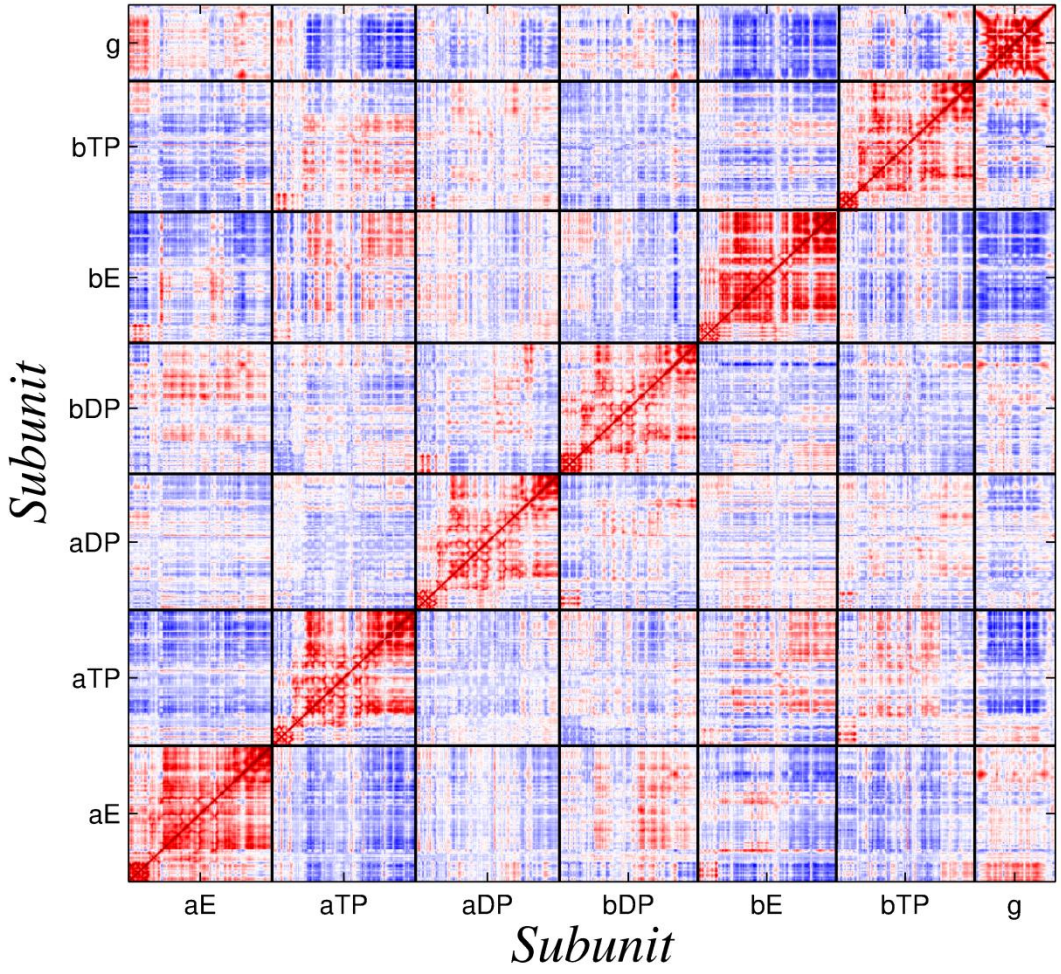

Figure S8

D)

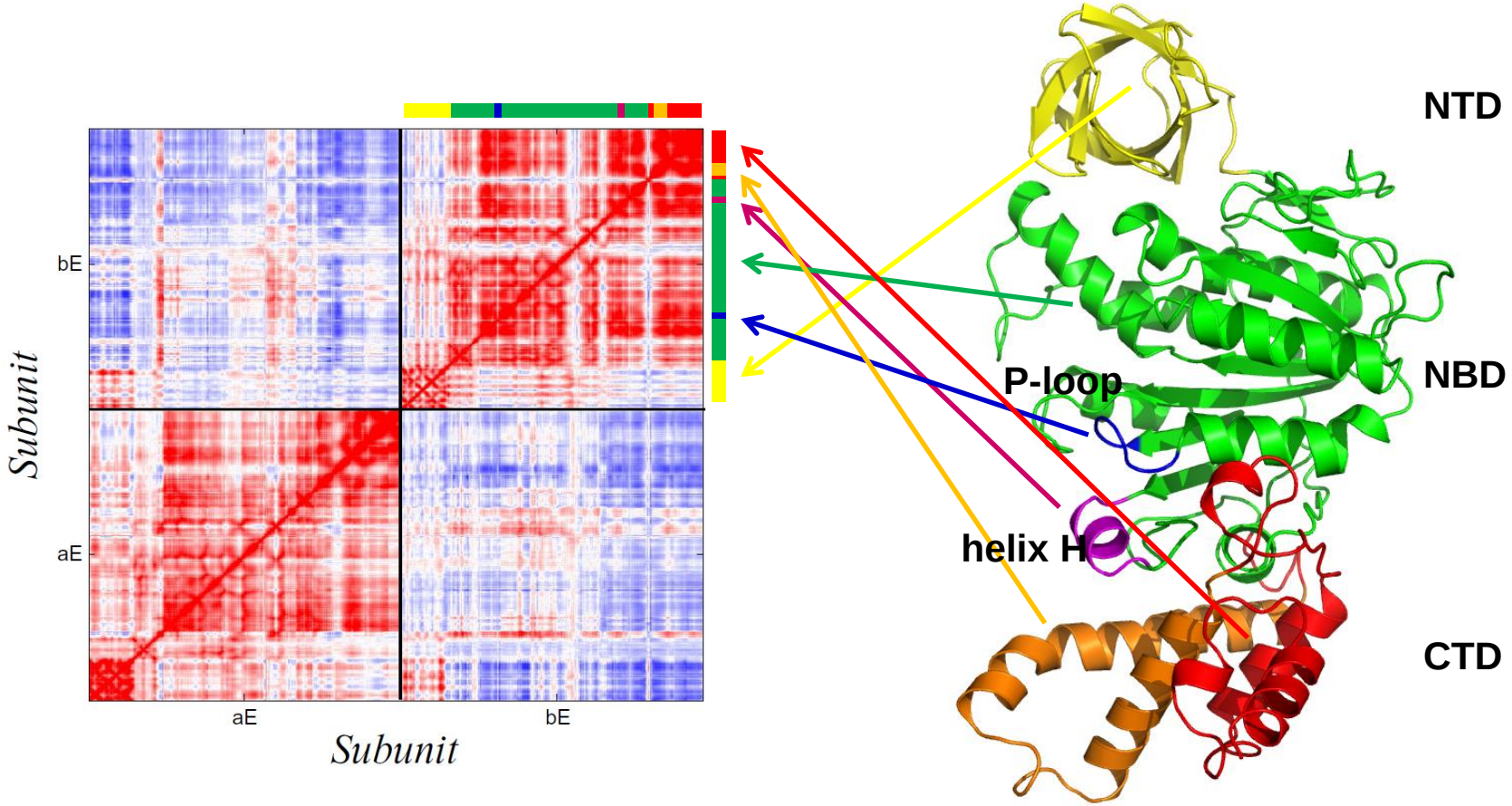

Figure S9

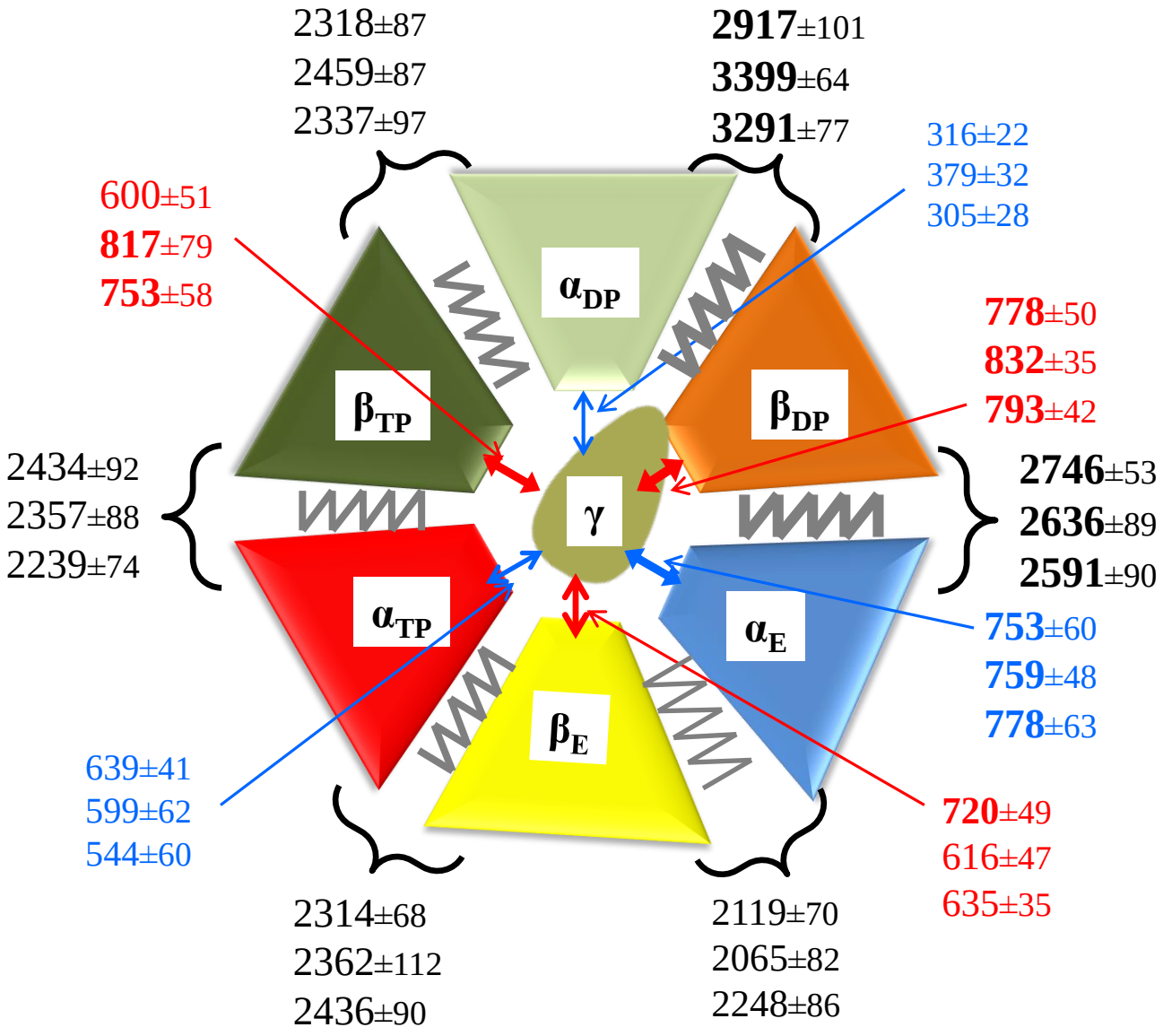
2318±87
2459±87
2337±97
2917±101
3399±64
3291±77
316±22
379±32
305±28
600±51
817±79
753±58
778±50
832±35
793±42
2434±92
2357±88
2239±74
2746±53
2636±89
2591±90
753±60
759±48
778±63
639±41
599±62
544±60
720±49
616±47
635±35
2314±68
2362±112
2436±90
2119±70
2065±82
2248±86
αDP
βDP
βTP
γ
αTP
αE
βE

Figure S10

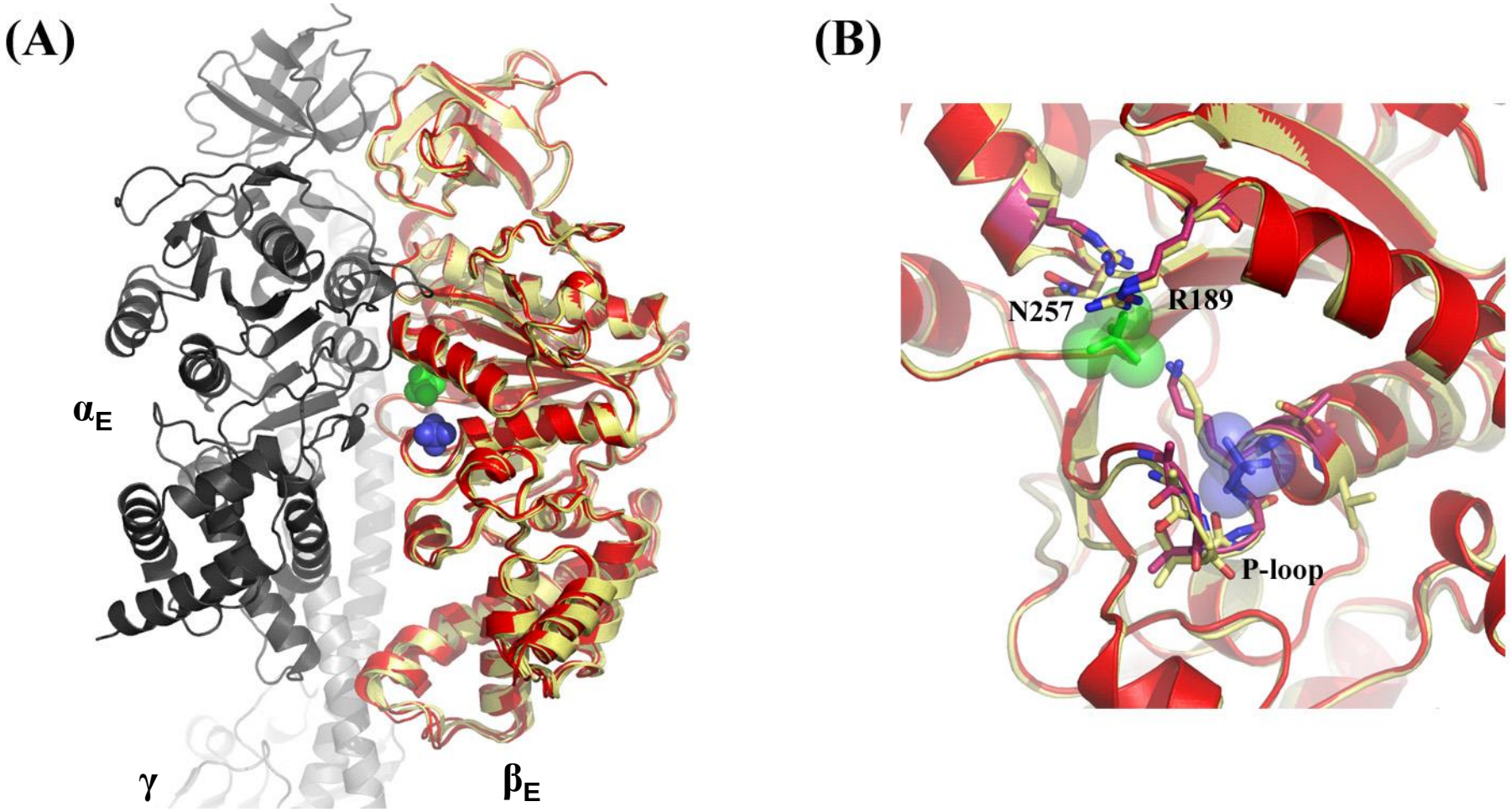

Figure S11

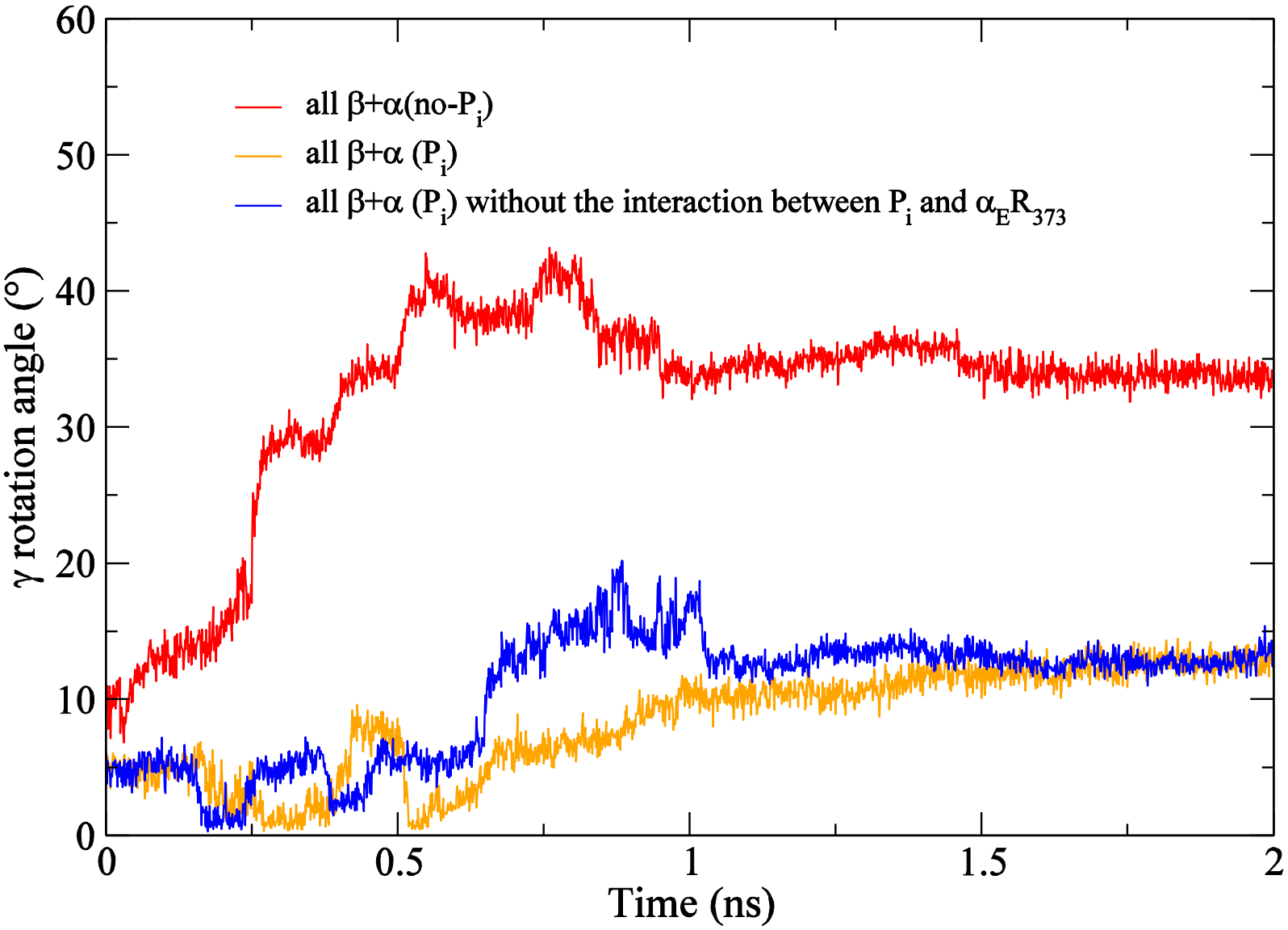
all β+α(no-P$_i$)
all β+α (P$_i$)
all β+α (P$_i$) without the interaction between P$_i$ and α$_E$R$_{373}$
γ rotation angle (°)
Time (ns)
0
10
20
30
40
50
60
0
0.5
1
1.5
2

Figure S12

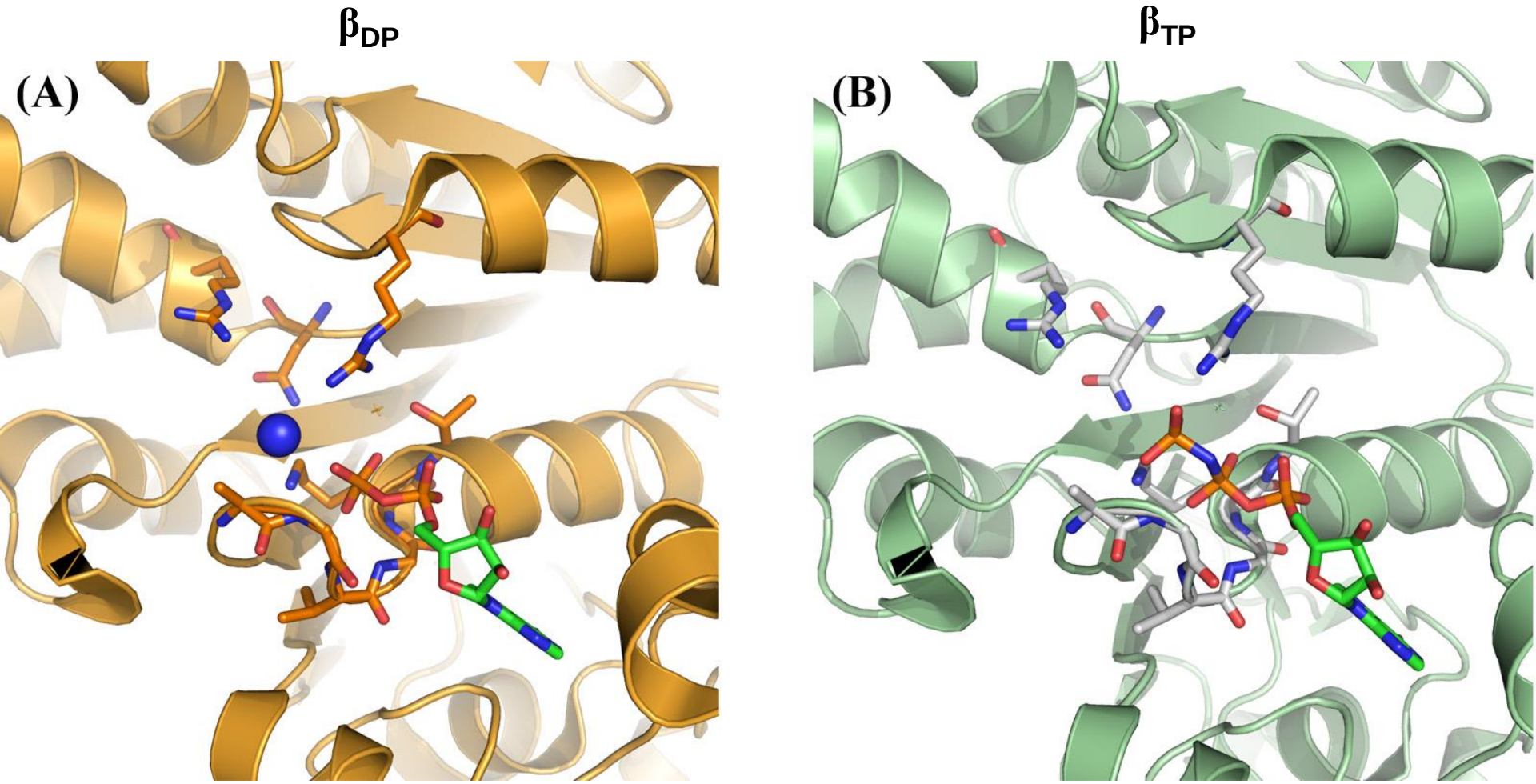

Figure S13

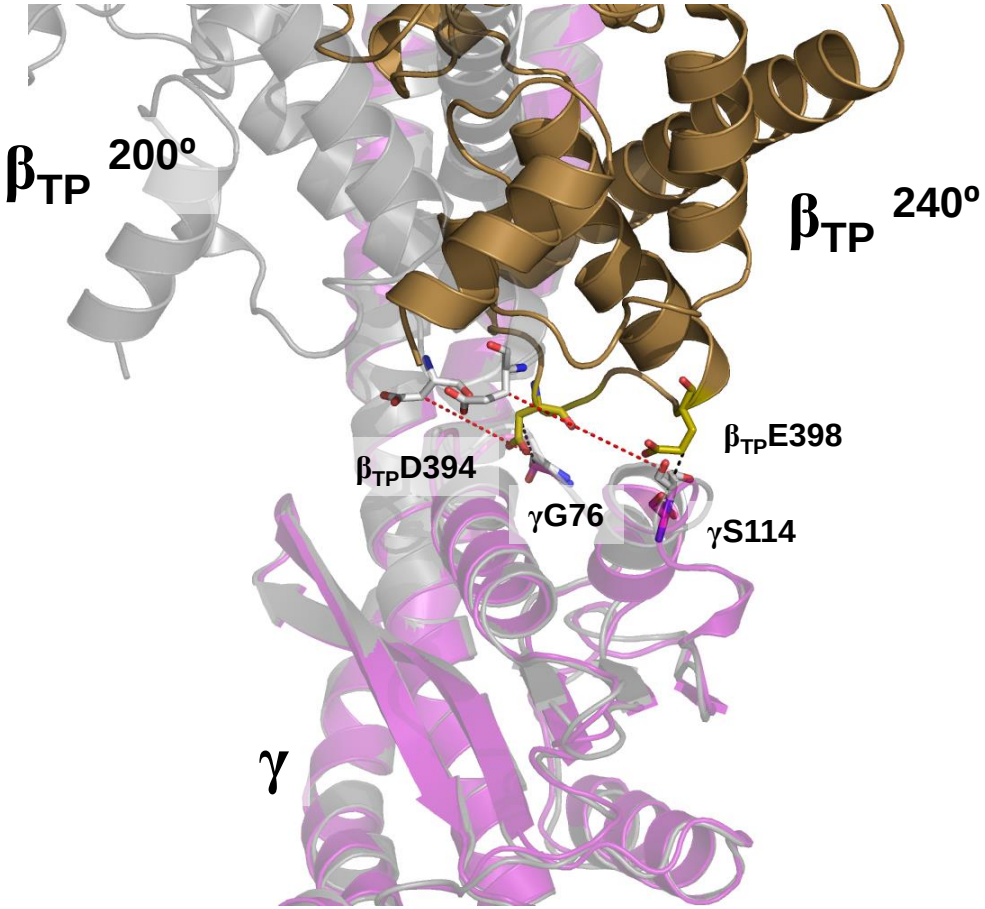

240º/200º